Brain Structure and Function (2020) 225:1135–1152
https://doi.org/10.1007/s00429-020-02065-y

ORIGINAL ARTICLE

GABAergic and non-GABAergic subpopulations of Kv3.1b-expressing neurons in macaque V2 and MT: laminar distributions and proportion of total neuronal population

Jenna G. Kelly[1] · **Michael J. Hawken**[1]

Received: 5 September 2019 / Accepted: 27 March 2020 / Published online: 7 April 2020

Abstract

The Kv3.1b potassium channel subunit, which facilitates the fast-spiking phenotype characteristic of parvalbumin (PV)-expressing inhibitory interneurons, is also expressed by subpopulations of excitatory neurons in macaque cortex. We have previously shown that V1 neurons expressing Kv3.1b but not PV or GABA were largely concentrated within layers 4Cα and 4B of V1, suggesting laminar or pathway specificity. In the current study, the distribution and pattern of co-immunoreactivity of GABA, PV, and Kv3.1b across layers in extrastriate cortical areas V2 and MT of the macaque monkey were measured using the same triple immunofluorescence labeling, confocal microscopy, and partially automated cell-counting strategies used in V1. For comparison, densities of the overall cell and neuronal populations were also measured for each layer of V2 and MT using tissue sections immunofluorescence labeled for the pan-neuronal marker NeuN. GABAergic neurons accounted for 14% of the total neuronal population in V2 and 25% in MT. Neurons expressing Kv3.1b but neither GABA nor PV were present in both areas. This subpopulation was most prevalent in the lowest subcompartment of layer 3, comprising 5% of the total neuronal population in layer 3C of both areas, and 41% and 36% of all Kv3.1b+ neurons in this layer in V2 and MT, respectively. The prevalence and laminar distribution of this subpopulation were remarkably consistent between V2 and MT and showed a striking similarity to the patterns observed previously in V1, suggesting a common contribution to the cortical circuit across areas.

Keywords Extrastriate cortex · Kv3.1b · Neuronal density · GABA · Parvalbumin

Introduction

The neocortex is comprised of anatomically and functionally diverse cell types with distinct contributions to cortical circuits. A full understanding of the mechanisms by which cortical circuits function will require a detailed knowledge of the diversity of cell types, their position within the cortical architecture, and their different functional properties. It is, furthermore, essential to identify the differences in organization and cellular composition between species and cortical areas and to understand how such differences specifically impact function. Connectivity, parcellation, and composition of the neocortex each differ between species (Preuss 2001; De Felipe et al. 2002), and while many cell types defined by expression of molecular markers appear to be conserved across species, corresponding cell types can differ in distribution (De Felipe et al. 2002; Hof and Sherwood 2005; Sherwood et al. 2007; Zeng et al. 2012), intrinsic physiology (Povysheva et al. 2007, 2008), and co-expression of other genes and/or proteins (Zeng et al. 2012; Disney and Reynolds 2014; Coppola and Disney 2018) across species and brain areas.

In multiple cortical areas in the macaque monkey, subsets of pyramidal and non-GABAergic neurons express the Kv3.1b potassium channel subunit (Härtig et al. 1999; Ichinohe et al. 2004; Constantinople et al. 2009; Soares et al. 2017; Kelly et al. 2019). This channel type, which functionally subserves the fast-spiking phenotype (Du et al. 1996; Wang et al. 1998; Erisir et al. 1999; Rudy et al. 1999)

Electronic supplementary material The online version of this article (https://doi.org/10.1007/s00429-020-02065-y) contains supplementary material, which is available to authorized users.

✉ Michael J. Hawken
mjh2@nyu.edu

[1] Center for Neural Science, New York University, 4 Washington Place, New York, NY 10003, USA

characteristic of parvalbumin (PV)-expressing interneurons (Kawaguchi and Kubota 1993, 1998; Cauli et al. 1997), is almost entirely co-expressed with PV in rodent neocortex (Weiser et al. 1995; Du et al. 1996; Chow et al. 1999; Hernández-Pineda et al. 1999; Rudy et al. 1999). In macaque motor and premotor cortex, large pyramidal neurons have been shown to exhibit narrow spike waveforms, suggesting a dissociation of this physiological phenotype from PV interneurons in the primate (Vigneswaran et al. 2011); notably, this set of electrophysiologically identified neurons included the Betz cells, which express Kv3.1b (Ichinohe et al. 2004; Soares et al. 2017).

We have recently shown that Kv3.1b-expressing excitatory neurons in V1 are largely compartmentalized within layers 4Cα and 4B, in addition to the noteworthy inclusion of the large Meynert cells at the layer 5/6 border (Kelly et al. 2019). Although Kv3.1b-immunoreactive (subsequently styled "Kv3.1b+") pyramidal and non-GABAergic neurons have been described in V1 (Constantinople et al. 2009; Kelly et al. 2019), V2 (Ichinohe et al. 2004), and premotor, motor, and parietal cortical areas (Härtig et al. 1999; Ichinohe et al. 2004; Soares et al. 2017), the laminar distribution of Kv3.1b+/GABA−/PV− neurons had not been quantified in extrastriate visual cortical areas. We identified putative Kv3.1b+ excitatory neurons in areas V2 and MT and measured their laminar distribution using the combination of triple immunofluorescence labeling, sampling, and partially automated cell-counting strategies used previously in V1 (Kelly et al. 2019). Our results suggest that Kv3.1+ excitatory subpopulations in extrastriate cortex exhibit laminar specificity similar to that observed in V1.

In addition to identifying Kv3.1b+/GABA−/PV− neurons, labeling for GABA and PV also allowed us to quantitatively describe the laminar distributions of GABAergic and PV+ subpopulations in V2 and MT, revealing both common organizational patterns and differences across cortical areas. Laminar densities of the overall neuronal populations were also measured using immunohistochemistry for NeuN (Mullen et al. 1992; Wolf et al. 1996; Kelly and Hawken 2017; Kelly et al. 2019) to allow area-specific comparisons with the specific subpopulations.

Materials and methods

Macaque tissue

Tissue samples were from five macaque monkeys (two male *Macaca fascicularis*, M1-2, aged 5.8 and 4.8 years; one male *M. mulatta*, M3, aged 7.5 years; one female *M. nemestrina*, M4, aged 2.6 years; and one male *M. nemestrina,* M5, aged 6.8 years) that were previously used for anesthetized electrophysiological experiments (Goris et al. 2015; Ziemba et al. 2018, 2019). After 5–6 days of acute electrophysiological recording, experiments were terminated by intravenous injection of a lethal dose of pentobarbital (60 mg/kg), and brain death was determined by a flat electroencephalogram. Each animal was perfused transcardially with cold heparinized 0.01 M phosphate-buffered saline (PBS, pH 7.3), followed by 4% paraformaldehyde (PFA) plus 0.125% glutaraldehyde in 0.1 M phosphate buffer (PB, pH 7.4). Extracted brain tissue was blocked and post-fixed overnight in 4% PFA at 4 °C before vibratome sectioning. Blocks containing areas V1 and V2 were cut into serial 50 µm parasagittal sections. Blocks containing area MT were cut into serial 50 µm coronal sections. After sectioning, tissue was rinsed with 1% sodium borohydride in 0.1 M PB to reduce the antigen masking effects of glutaraldehyde. All sections were immersed in graded sucrose solutions to prepare them for freezing and then stored in cryoprotectant solution at − 20 °C until the time of immunohistochemical processing.

Immunofluorescence labeling

Free-floating sections were triple immunofluorescence labeled using the same antibodies and protocols described previously (Kelly and Hawken 2017; Kelly et al. 2019). First, to counteract the antigen masking effects associated with aldehyde fixation (Shi et al. 1991), sections were incubated in a sodium citrate buffer solution (3.8% citric acid, 2.4% sodium citrate; pH 8.0) for 15 min in an 80 °C water bath, followed by 20 min at room temperature (García-Marín et al. 2013). We then followed a protocol adapted from the iDISCO method (Renier et al. 2014), which we have found to improve antibody penetration. Sections were dehydrated in 0%, 50%, 80% and twice in 100% methanol/0.01 M phosphate-buffered saline (PBS) for 30 min each, chilled over ice, and bleached in 5% hydrogen peroxide/20% DMSO/methanol at 4 °C overnight. They were rinsed twice in 100% methanol for 30 min each, incubated in 20% DMSO/methanol for 1 h, and rehydrated in 80%, 50%, and 0% methanol/PBS. They were incubated twice in 0.3% Triton-X/PBS for 30 min at room temperature, and then incubated for 2 h at 37 °C in 0.3% Triton-X/20% DMSO/0.3 M glycine/PBS. Sections were blocked for 2 h at 37 °C in 0.3% Triton-X/10% DMSO/6% NGS/PBS, rinsed twice in 0.2% Tween-20/PBS with 10 µg/mL heparin (PTwH) for 30 min each, and incubated for 3 days at 4 °C with rabbit anti-GABA polyclonal serum (1:1000; 20 094, Immunostar, Hudson, WI, USA) diluted in 3% NGS/PTwH. Sections were rinsed three times in PTwH and then incubated overnight at 4 °C with Alexa Fluor® 594 goat anti-rabbit IgG (H + L) antibody (1:2000; A-11 012, Invitrogen, Carlsbad, CA, USA) in 3% NGS/PTwH. The same antibody incubation steps were repeated for the remaining antibodies: mouse anti-Kv3.1b monoclonal serum (1:250; Antibodies Incorporated, Davis,

CA, USA), Alexa Fluor® 488 goat anti-mouse IgG (H + L) antibody (1:2000; A-11 001, Invitrogen), guinea pig anti-PV polyclonal serum (1:1000; 195 004, Synaptic Systems, Göttingen, Germany) or guinea pig anti-NeuN (1:1000; ABN90P, Millipore, Billerica, MA, USA), and biotinylated goat anti-guinea pig IgG (1:500; BA-7000, Vector, Burlingame, CA, USA). Sections were then rinsed and incubated overnight in solution containing Alexa Fluor® 647 streptavidin conjugate antibody (1:2000; S-32 357, Invitrogen). After a final three rinses in PBS, sections were treated according to the manufacturer's protocol with Autofluorescence Eliminator Reagent (2160, Millipore, Billerica, MA, USA) to minimize lipofuscin-like autofluorescence, counterstained with 10 µg/mL DAPI, and mounted in ProLong Gold Antifade Reagent (P-36 930, Invitrogen).

Sampling of V2 and MT

The distribution of Kv3.1b, PV, and GABA in V2 was measured from sections that contained both opercular V1 and dorsal V2, which were immunolabeled to measure the distribution of these antigens in V1 in a previous study (Kelly et al. 2019). The transition from V1 to V2 was clearly identifiable based on the characteristic subdivision of layer 4 in V1. One sample was obtained from an approximate distance of 1.5 mm from this boundary, and the rest were obtained from the posterior bank of the lunate sulcus. The sampled regions are thus expected to correspond to the representation of the parafoveal lower visual field similar to the sampled regions in V1 (Kelly et al. 2019), and they are well matched to the samples from which total neuronal density estimates were made (Kelly and Hawken 2017). The laminar densities of neurons identified with NeuN are from the data set presented in Kelly and Hawken (2017) but have here been separated by layer for comparison with the densities of specific subtypes.

MT blocks typically began slightly anterior to the posterior end of the lateral sulcus and were bounded at their posterior end at or just anterior to the lunate sulcus. The location of area MT on the posterior bank of the superior temporal sulcus was identified by comparison of sections with macaque brain atlases and by processing every 10–20 sections using a modification of the Gallyas method (Pistorio et al. 2006) to reveal the dense myelination associated with MT. Additional sections were processed for SMI-32 (Hof and Morrison 1995) or cytochrome oxidase (Wong-Riley 1979; Horton 1984; Tootell and Taylor 1995) to differentiate MT from neighboring areas. We did not attempt to target a specific topographic location; it is likely that the MT samples included the representation of higher eccentricities relative to the V1 and V2 samples, and they likely included both the upper and lower visual quadrants. By comparison of our tissue sections (Supplementary Fig. 1) against an annotated rhesus macaque atlas (Saleem and Logothetis 2007), we estimate that samples from one animal (M2) were from the anterior-most 3 mm of MT, corresponding to the representation of the fovea and parafovea (Desimone and Ungerleider 1986), while the samples from the other three animals come from a more posterior region of MT and most likely correspond to the representation of the parafoveal and peripheral visual field. Because the borders of MT can be ambiguous to identify (Maunsell and Van Essen 1983), we avoided border regions when sampling.

In both areas, V2 and MT, sample regions were strips of tissue spanning from the pial surface to the white matter perpendicular to the pial surface within a section (Kelly and Hawken 2017). Samples were acquired from regions with apparently uniform quality of antibody label over the full span from the pial surface to the white matter, avoiding tears in the tissue but not blood vessels. The scan field was rotated to the axis perpendicular to the pattern of cortical layers. A series of overlapping *z* stacks was acquired, beginning with a stack that included the pial surface and ending with a *z* stack containing the layer 6/white matter boundary.

Image acquisition

Sections were imaged using either a Leica TCS SP5 or SP8 confocal system (Leica Microsystems, Wetzlar, Germany). DAPI and fluorophores conjugated to different antibodies were each excited independently in wavelength-separated channels. A 488 nm Argon laser, a 561 nm DPSS laser, and a 633 He–Ne laser were used to excite the Kv3.1b-, GABA-, and PV- or NeuN-conjugated fluorophores, respectively, and a 405 nm UV diode laser was used to excite DAPI. PMT detection/wavelength selection windows were adjusted such that each laser/fluorophore's emissions were detected only in the appropriate channel. Gain and offset levels for channels with strong signal to noise (DAPI, NeuN, and PV) were set such that bright labeled regions in preview scan images were at saturation and there was minimal background fluorescence signal. For GABA and Kv3.1b, gain and offset levels were set to preserve the range of intensity levels: few pixels were allowed to saturate, and only the regions that should have been truly devoid of signal—regions within blood vessels or above the pial surface—fell under the low-intensity offset level. Image stacks were acquired by specifying an upper and lower *z* position and acquiring images of each channel sequentially, with scanning speed 200 Hz (DAPI/Kv3.1b/GABA/PV) or 400 Hz (DAPI/NeuN), *z* step size 0.5 µm, pinhole size 1 airy unit, and refraction index 1.5. Most images were acquired using the SP5 confocal system, using a 63 × oil-immersion objective lens (NA 1.4), with no digital zoom applied. The remainder, acquired with the SP8 confocal system, used a 40 × oil-immersion objective lens (NA 1.3) with a digital zoom of 1.18 × to approximately match

voxel size across samples. The (*x*–*y*) image resolution per frame was 1024 × 1024 pixels (246 µm × 246 µm), yielding an effective voxel size of 241 × 241 × 502–503.5 nm.

Image stack volume depended on penetration of the antibody into the tissue. For most of the DAPI/NeuN image series sampled to measure overall neuronal density, there was complete or nearly complete antibody penetration, so image stacks spanned the full depth of the tissue, with upper and lower *z* limits just above and below (respectively) the cut surfaces of the tissue. In some cases when antibody penetration was very limited, one image stack *z* limit was specified a few µm above the cut surface of the tissue (outside the section), and the other *z* limit was specified several µm past the limit of antibody penetration in the channel for which this was most limiting (typically GABA). In these cases, after every second *z* stack an additional image stack containing only the DAPI channel was acquired with a 1 µm *z* step and upper and lower *z* limits specified above and below the cut surfaces of the tissue. This allowed estimation of tissue shrinkage in the *z* dimension.

To measure the distribution and co-expression of Kv3.1b, GABA, and PV in V2, a total of 13 series were acquired, with at least three series and a total thickness (*z* distance) of 39–70 µm from each of three animals (M1-3). The total thickness sampled was 162 µm. To measure the distribution and co-expression of Kv3.1b, GABA, and PV in MT, a total of 16 series were acquired, with at least three series and a total thickness of 39–62 µm from each of three animals (M2, M4, M5). The total thickness sampled was 156 µm. To measure the overall neuronal population in MT, a total of 12 series were acquired for the DAPI and NeuN channels, with at least three series and a total thickness of 58–100 µm from each of three animals (M2–4). The total thickness sampled was 232 µm.

Cell counting and classification

DAPI image stacks were automatically analyzed to identify the 3D centroids of cell nuclei (Kelly and Hawken 2017). The full set of identified nuclei in each stack was restricted to a specialized 3D counting volume adapted from the counting box/counting brick (Howard et al. 1985; Williams and Rakic 1988), described in detail in Kelly and Hawken (2017). The DAPI-labeled nuclei remaining after applying the exclusion boundaries were classified by determining whether there was immunolabeling for any combination of the antigens of interest in a region surrounding the 3D DAPI centroid. This was done by creating binary mask images for each channel that had solid positive regions inside the labeled area for each cell and zeros elsewhere, and then evaluating the proportion of positive pixels in a circular region centered on the DAPI centroid (Kelly and Hawken 2017; Kelly et al. 2019). For Kv3.1b/GABA/PV series, classification was first performed automatically and then corrected manually, as described in Kelly et al. (2019).

Cell positions were registered across stacks in a given series and converted to cell density as a function of normalized cortical depth as described previously (Kelly and Hawken 2017; Kelly et al. 2019). The amount of tissue shrinkage due to tissue processing was determined for each series and applied to the measurements for that series. Tissue shrinkage in the *z* dimension was quantified by measuring the distance from the top to the bottom of the mounted tissue (mean measured distance: 32.0 µm ± 1.6 µm SEM, $N = 13$ for the study of Kv3.1b, GABA, and PV in V2; 35.6 µm ± 1.7 µm SEM, $N = 16$ for Kv3.1b, GABA, and PV in MT; and 37.0 µm ± 2.2 µm SEM, $N = 12$ for total neuronal density in MT) and comparing this to the 50 µm thickness of each section at the time of sectioning. The degree of shrinkage in the plane of section (*x* and *y* dimensions) was estimated for each series in the region sampled by identifying the same blood vessels in the processed section and in a micrograph of the same section imaged prior to immunolabeling using an Olympus VS120-FL virtual slide scanning system. For 7 out of 41 series, the sections were not scanned prior to immunolabeling, so *x* and *y* shrinkage was estimated by comparison to unlabeled adjacent sections. The extent from the pial surface to the white matter (*y* length) at the locations of blood vessel landmarks and the horizontal (*x*) lengths between landmarks at the level of the stria of Gennari were measured from images acquired before and after immunolabeling. The mean *x* and *y* length measurements in local regions surrounding the sampled sites were used to estimate the degree of shrinkage in these dimensions. Across V2 samples, the mean shrinkage in *x* was 21%, while the mean shrinkage in *y* was 15%; that is, the original size in the *x* dimension was 1.27 times the size after processing, while the original size in the *y* dimension was 1.18 times the size after processing. For MT samples stained for NeuN, the mean shrinkage in *x* was 18%, and the mean shrinkage in *y* was 16%. For MT samples stained for GABA, PV, and Kv3.1b, the mean shrinkage in *x* was 19%, and the mean shrinkage in *y* was 14%.

Computing laminar densities

For each image series, the numbers of nuclei and of each type of neuron were also measured within each laminar compartment. The volume per layer was measured as the distance between that layer's upper and lower boundary converted to µm, multiplied by the width of the image stacks (*x* dimension) times the sampled distance in the *z* dimension, corrected for tissue shrinkage. Laminar boundaries were identified separately for each sampled image series by identifying transitions in density of DAPI-labeled nuclei as well as NeuN-labeled neurons, when available. The boundary

between layers 1 and 2 was demarcated as the point of abrupt transition from a general absence of nuclei to a highly packed strip of nuclei. Layer 4 was identified as a strip of relatively uniform and densely packed nuclei. The layer 5–6 border was marked by a higher nuclear density in the upper part of layer 6 compared to layer 5. The layer 6-white matter transition was identified based on an abrupt decrease in PV-labeled processes, which were largely absent in the white matter, or of neurons, and by the presence of many nuclei with dense, apparently uniform chromatin staining.

Across studies, there are discrepancies in the assignment of laminar and sublaminar boundaries of layers 2 and 3; in many studies, no attempt is made to subdivide these layers. Following the descriptions of von Economo (1927) and Bonin and Bailey (1947), we have divided layers 2 and 3 into four subcompartments, designated layers 2, 3A, 3B, and 3C. Layer 2 was identified as a region of small, densely packed cells. As described by von Economo (1927), the boundary between layers 2 and 3A is not starkly visible. We have defined layer 2 as a restricted region of particularly high cell density (von Economo 1927; Rockland and Pandya 1979; Balaram and Kaas 2014), although some authors have included in layer 2 part of what we have designated layer 3A (e.g. Valverde 1978; Lund et al. 1981; Balaram et al. 2014). Layer 3 was divided into three subcompartments (3A, 3B, and 3C; Von Economo 1927), although these boundaries were difficult to identify, particularly in the absence of NeuN immunolabeling. Layer 3A typically had a high cell density compared to layers 3B and 3C. Layer 3B was devoid of the large pyramidal cells typical of layer 3C and often appeared lower in cell density.

In the current study, layer 3C approximately corresponds to layer 3B of Lund et al. (1981) and Valverde (1978); layers 3B and 3C together approximately correspond to a single larger sublayer designated 3B in Balaram et al. (2014). The precise boundaries of layer 2/3 subcompartments are not especially critical to the interpretation of the current results, except to the extent that comparable boundaries have been identified when measuring total neuronal density and densities of Kv3.1b+, PV+, and GABA+ subpopulations. The similarity in cell densities and in the average fraction of the cortical depth occupied by each sublayer (shown in Table 1 for V2 and in Table 2 for MT) suggests this is the case.

Laminar boundaries are not always cleanly delimited as horizontal lines, particularly when different laminar boundaries within a column are not perfectly parallel to each other or when a boundary is not characterized by a starkly visible difference in cell composition. In all data presented below, laminar boundaries have been established as horizontal lines through the image stacks, and no exclusion zones have been implemented surrounding these boundaries. Therefore, density estimates for each layer likely show some contamination by neighboring layers. For interested readers, analogs of Tables 1, 2, 3, 4 are included as Supplementary Tables 1–4 using instead the central one-third of the vertical (radial) length of each layer to compute densities.

Image processing for figures

ImageJ (Rasband WS, ImageJ, U. S. National Institutes of Health, Bethesda, Maryland, USA, https://imagej.nih.gov/ij/, 1997–2018) was used to adjust image brightness and contrast levels of micrographs presented in figures and to generate pseudocolored overlays of multiple channels.

Table 1 Total cell and neuronal densities in each layer of V2

Layer	Total cell density	Measured neuronal density	Fraction of cortical depth	NeuN/DAPI	Total cell density	Estimated neuronal density	Fraction of cortical depth
1	90.8 ± 4.3	11.8 ± 1.7	0.11	0.13	91.4 ± 10.6	11.8 ± 1.4	0.12
2	245.1 ± 4.4	201.6 ± 4.7	0.07	0.82	238.3 ± 8.8	196.0 ± 7.3	0.06
3A	205.0 ± 8.3	151.1 ± 4.5	0.13	0.74	219.9 ± 4.1	162.3 ± 3.0	0.13
3B	182.7 ± 8.8	116.2 ± 5.4	0.13	0.64	184.0 ± 2.7	117.0 ± 1.7	0.15
3C	213.1 ± 19.6	131.0 ± 10.6	0.14	0.62	203.0 ± 13.0	125.0 ± 8.0	0.14
4	351.3 ± 36.5	255.9 ± 21.7	0.10	0.73	333.6 ± 16.6	244.0 ± 12.1	0.10
5	207.1 ± 15.5	131.2 ± 11.0	0.15	0.63	203.3 ± 6.3	128.6 ± 4.0	0.14
6	183.5 ± 8.3	91.5 ± 7.6	0.17	0.50	191.1 ± 6.6	95.0 ± 3.3	0.15
1–6	205.0 ± 12.3	129.5 ± 8.0	1.00	0.63	201.7 ± 5.0	127.4 ± 3.2	1.00

Densities are presented as means (in thousands) ± SEM ($N = 3$). Column 1: cortical layer or sublayer. Column 2: total density of DAPI-labeled cells in the NeuN-labeled series. Column 3: total neuronal density in the NeuN-labeled series. Column 4: span of the layer in the direction normal to the cortical surface, as a fraction of the total depth from the pial surface to white matter, in the NeuN-labeled series. Column 5: the ratio of neurons to the overall cell population in the layer. Column 6: total density of DAPI-labeled cells in the Kv3.1b/PV/GABA-labeled series. Column 7: total neuronal density in the Kv3.1b/PV/GABA-labeled series estimated using the total cell density and the NeuN/DAPI ratio measured in the NeuN-labeled series. Column 8: relative cortical depth occupied by the layer in the Kv3.1b/PV/GABA-labeled series

Table 2 Total cell and neuronal densities in each layer of MT

Layer	Total cell density	Measured neuronal density	Fraction of cortical depth	NeuN/DAPI	Total cell density	Estimated neuronal density	Fraction of cortical depth
1	113.5 ± 22.3	22.5 ± 4.3	0.08	0.20	104.0 ± 12.1	20.8 ± 2.4	0.09
2	243.2 ± 50.9	185.3 ± 42.1	0.05	0.76	258.2 ± 28.8	195.4 ± 21.8	0.06
3A	187.2 ± 31.5	128.2 ± 23.6	0.11	0.68	194.8 ± 8.3	132.9 ± 5.7	0.10
3B	174.3 ± 26.5	92.5 ± 16.2	0.14	0.53	170.0 ± 10.0	89.7 ± 5.3	0.13
3C	201.0 ± 32.9	106.0 ± 17.2	0.14	0.53	200.3 ± 6.2	105.9 ± 3.3	0.14
4	267.1 ± 37.8	176.8 ± 24.2	0.12	0.66	262.3 ± 20.8	174.0 ± 13.8	0.12
5	173.3 ± 20.9	93.3 ± 9.8	0.17	0.54	167.7 ± 6.3	90.7 ± 3.4	0.16
6	152.5 ± 11.0	73.5 ± 2.9	0.20	0.48	152.5 ± 11.3	73.8 ± 5.5	0.21
1–6	183.5 ± 23.6	102.9 ± 12.2	1.00	0.56	182.2 ± 8.8	102.6 ± 5.0	1.00

Densities are presented as means (in thousands) ± SEM ($N = 3$). Column 1: cortical layer or sublayer. Column 2: total density of DAPI-labeled cells in the NeuN-labeled series. Column 3: total neuronal density in the NeuN-labeled series. Column 4: span of the layer in the direction normal to the cortical surface, as a fraction of the total depth from the pial surface to white matter, in the NeuN-labeled series. Column 5: the ratio of neurons to the overall cell population in the layer. Column 6: total density of DAPI-labeled cells in the Kv3.1b/PV/GABA-labeled series. Column 7: total neuronal density in the Kv3.1b/PV/GABA-labeled series estimated using the total cell density and the NeuN/DAPI ratio measured in the NeuN-labeled series. Column 8: relative cortical depth occupied by the layer in the Kv3.1b/PV/GABA-labeled series

Table 3 Laminar densities of different neuronal subpopulations in V2

Layer	Kv3.1b−, PV−, GABA+ (% Neurons)	Kv3.1b+, PV−, GABA− (% Neurons)	Kv3.1b−, PV+, GABA− (% Neurons)	Kv3.1b+, PV−, GABA+ (% Neurons)	Kv3.1b−, PV+, GABA+ (% Neurons)	Kv3.1b+, PV+, GABA− (% Neurons)	Kv3.1b+, PV+, GABA+ (% Neurons)
1	8.7 ± 1.1 (73%)	0.0 ± 0.0 (0%)	0.0 ± 0.0 (0%)	0.0 ± 0.0 (0%)	0.2 ± 0.2 (1%)	0.0 ± 0.0 (0%)	0.0 ± 0.0 (0%)
2	17.1 ± 1.9 (9%)	0.2 ± 0.2 (0%)	0.3 ± 0.3 (0%)	0.9 ± 0.4 (0%)	0.2 ± 0.2 (0%)	1.1 ± 0.8 (1%)	2.2 ± 0.7 (1%)
3A	16.8 ± 2.0 (10%)	0.8 ± 0.2 (0%)	0.2 ± 0.2 (0%)	2.7 ± 0.5 (2%)	0.8 ± 0.2 (0%)	0.6 ± 0.4 (0%)	6.5 ± 1.2 (4%)
3B	9.3 ± 1.9 (8%)	0.9 ± 0.1 (1%)	0.6 ± 0.6 (1%)	0.4 ± 0.2 (0%)	0.7 ± 0.2 (1%)	1.0 ± 0.2 (1%)	6.4 ± 1.8 (5%)
3C	8.6 ± 1.5 (7%)	6.6 ± 1.6 (5%)	0.0 ± 0.0 (0%)	0.4 ± 0.3 (0%)	0.6 ± 0.1 (1%)	1.0 ± 0.7 (1%)	8.0 ± 1.2 (6%)
4	9.3 ± 2.2 (4%)	1.1 ± 0.3 (0%)	0.8 ± 0.3 (0%)	0.2 ± 0.2 (0%)	0.6 ± 0.6 (0%)	2.3 ± 1.1 (1%)	19.6 ± 1.0 (8%)
5	6.8 ± 2.5 (5%)	0.7 ± 0.6 (1%)	0.8 ± 0.8 (1%)	0.1 ± 0.1 (0%)	0.8 ± 0.3 (1%)	0.1 ± 0.1 (0%)	8.0 ± 0.6 (6%)
6	5.7 ± 0.8 (6%)	0.5 ± 0.3 (1%)	0.3 ± 0.3 (0%)	0.0 ± 0.0 (0%)	0.3 ± 0.2 (0%)	0.2 ± 0.2 (0%)	3.4 ± 0.7 (4%)
1–6	9.6 ± 1.1 (8%)	1.5 ± 0.3 (1%)	0.4 ± 0.3 (0%)	0.6 ± 0.2 (0%)	0.6 ± 0.1 (0%)	0.7 ± 0.3 (1%)	6.7 ± 0.3 (5%)

Laminar densities of neurons with each combination of Kv3.1b, PV, and GABA immunoreactivity are presented as means (in thousands) ± SEM ($N = 3$). Values in parentheses are the proportion of the total neuronal population in V2 accounted for by that cell type. Column 1: cortical layer or sublayer. Column 2: neurons immunoreactive only for GABA. Column 3: neurons immunoreactive only for Kv3.1b. Column 4: neurons immunoreactive only for PV. Column 5: Kv3.1b+/GABA+/PV− neurons. Column 6: Kv3.1b−/GABA+/PV+ neurons. Column 7: Kv3.1b+/PV+/GABA− neurons. Column 8: neurons immunoreactive for all three antigens

Results

The expression of Kv3.1b has been associated exclusively with inhibitory interneurons in rodent cortex (Weiser et al. 1995; Du et al. 1996; Chow et al. 1999; Hernández-Pineda et al. 1999; Rudy et al. 1999). However, in primate cortex substantial populations of putative excitatory neurons in multiple primate cortical areas have been found to be Kv3.1b+ (Härtig et al. 1999; Ichinohe et al. 2004; Constantinople et al. 2009; Soares et al. 2017; Kelly et al. 2019). In the current study we examined the distribution of Kv3.1b+/GABA−/PV− neurons in extrastriate visual cortical areas. We recently reported that in V1, Kv3.1b+/GABA−/PV− neurons were concentrated in layers 4B and 4Cα (Kelly et al. 2019). In the current study, parasagittal sections from dorsal V2 and coronal sections from MT were triple immunofluorescence labeled with anti-Kv3.1b, anti-PV, and anti-GABA and examined in series of confocal image stacks spanning the full cortical depth. This yielded the laminar distribution of neurons immunoreactive for Kv3.1b, PV, and GABA and allowed examination of their co-immunoreactivity patterns. As in V1 (Kelly et al. 2019), many Kv3.1b+ neurons in both V2 and MT were GABA+ and PV+ (Figs. 1, 2, arrowheads), but a substantial subpopulation were neither GABA+ nor PV+ (Figs. 1, 2, asterisks).

Table 4 Laminar Densities of Different Neuronal Subpopulations in MT

Layer	Kv3.1b−, PV−, GABA+ (% Neurons)	Kv3.1b+, PV−, GABA− (% Neurons)	Kv3.1b−, PV+, GABA− (% Neurons)	Kv3.1b+, PV−, GABA+ (% Neurons)	Kv3.1b−, PV+, GABA+ (% Neurons)	Kv3.1b+, PV+, GABA− (% Neurons)	Kv3.1b+, PV+, GABA+ (% Neurons)
1	16.1 ± 0.9 (80%)	0.0 ± 0.0 (0%)	0.0 ± 0.0 (0%)	1.1 ± 0.9 (5%)	0.0 ± 0.0 (0%)	0.0 ± 0.0 (0%)	0.9 ± 0.6 (4%)
2	39.4 ± 5.5 (21%)	0.3 ± 0.3 (0%)	0.0 ± 0.0 (0%)	2.8 ± 0.7 (2%)	0.4 ± 0.2 (0%)	0.0 ± 0.0 (0%)	5.4 ± 1.4 (3%)
3A	22.3 ± 3.7 (17%)	0.6 ± 0.2 (0%)	0.0 ± 0.0 (0%)	2.7 ± 1.0 (2%)	1.3 ± 0.2 (1%)	0.2 ± 0.2 (0%)	7.1 ± 0.9 (5%)
3B	13.2 ± 1.3 (15%)	1.3 ± 0.4 (2%)	0.2 ± 0.2 (0%)	1.2 ± 0.4 (1%)	0.4 ± 0.1 (0%)	0.7 ± 0.6 (1%)	7.6 ± 0.5 (9%)
3C	16.2 ± 4.2 (15%)	5.5 ± 0.8 (5%)	0.3 ± 0.1 (0%)	0.4 ± 0.2 (0%)	0.5 ± 0.3 (0%)	1.2 ± 0.3 (1%)	8.4 ± 1.2 (8%)
4	19.6 ± 5.7 (11%)	2.0 ± 0.9 (1%)	0.2 ± 0.2 (0%)	0.5 ± 0.2 (0%)	0.6 ± 0.6 (0%)	1.1 ± 0.1 (1%)	13.8 ± 1.0 (8%)
5	13.0 ± 4.2 (14%)	1.0 ± 0.3 (1%)	0.2 ± 0.1 (0%)	0.0 ± 0.0 (0%)	0.5 ± 0.2 (1%)	0.1 ± 0.1 (0%)	7.5 ± 0.2 (8%)
6	15.0 ± 1.6 (21%)	0.6 ± 0.2 (1%)	0.1 ± 0.1 (0%)	0.0 ± 0.0 (0%)	0.5 ± 0.3 (1%)	0.0 ± 0.0 (0%)	2.9 ± 0.5 (4%)
1–6	17.2 ± 2.6 (17%)	1.6 ± 0.3 (2%)	0.1 ± 0.0 (0%)	0.8 ± 0.2 (1%)	0.6 ± 0.1 (1%)	0.4 ± 0.1 (0%)	6.7 ± 0.6 (6%)

Laminar densities of neurons with each combination of Kv3.1b, PV, and GABA immunoreactivity are presented as means (in thousands) ± SEM ($N = 3$). Values in parentheses are the proportion of the total neuronal population in MT accounted for by that cell type. Column 1: cortical layer or sublayer. Column 2: neurons immunoreactive only for GABA. Column 3: neurons immunoreactive only for Kv3.1b. Column 4: neurons immunoreactive only for PV. Column 5: Kv3.1b+/GABA+/PV− neurons. Column 6: Kv3.1b−/GABA+/PV+ neurons. Column 7: Kv3.1b+/GABA−/PV+ neurons. Column 8: neurons immunoreactive for all three antigens

Total cell and neuronal density

Total cell and neuronal density varies greatly across cortical areas in primates (Collins et al. 2010; Collins 2011; Turner et al. 2016). Among visual areas, V1 has notably high neuronal densities (Rockel et al. 1980; Collins et al. 2010), macaque V2 has about half the neuronal density of V1 (Srinivasan et al. 2015; Kelly and Hawken 2017), and more anterior areas including MT have somewhat lower densities still (Collins et al. 2010). To compare the neuronal subpopulations labeled with Kv3.1b, PV, and/or GABA with the overall neuronal populations in each area and layer, we measured DAPI-labeled cell densities and NeuN-labeled neuronal densities using the automated counting method (Kelly and Hawken 2017). In MT, total cell density (184×10^3 cells per mm^3) and total neuronal density (103×10^3 neurons per mm^3) (Fig. 3) were slightly lower than in V2 (205×10^3 cells per mm^3, 130×10^3 neurons per mm^3; Kelly and Hawken 2017; Fig. 3). The ratio of neurons to cells was also slightly lower in MT (0.56) than in V2 (0.63). The ratio of neurons to cells varied across layers (Tables 1, 2) such that changes in density of non-neuronal cells did not follow changes in density of the total cell population across layers; in both areas, the density of non-neuronal cells was highest in layer 4 and lowest in layer 2, even though both layers 2 and 4 had higher neuronal and total cell densities compared to other layers.

Total cell densities were also measured in the Kv3.1b/PV/GABA-labeled samples. Overall cell densities and the densities in each cortical layer were very similar when measured from Kv3.1b/PV/GABA-labeled or NeuN-labeled samples from a given cortical area, suggesting that the densities measured from NeuN-labeled sections provide a reliable estimate of the total population in the samples used to measure specific neuronal subpopulations. The average total cell density across layers 1 through 6 measured from Kv3.1b/PV/GABA-labeled sections in V2 was 202×10^3 cells per mm^3, which was multiplied by the average ratio of neurons to cells to estimate that the density of neurons of all types in the sampled image series was 127×10^3 neurons per mm^3. In MT, the average total cell density across layers 1 through 6 measured from Kv3.1b/PV/GABA-labeled sections was 182×10^3 cells per mm^3, producing an estimated neuronal density of 103×10^3 neurons per mm^3. The same calculation was also applied to the cell density in each layer, using the ratio of neurons to all cell types specific to that layer (Tables 1, 2). The resulting estimates of total neuronal density were used to evaluate the laminar distribution of specific neuron types (e.g. Kv3.1b+ neurons) relative to the laminar distribution of the total neuronal population.

GABA immunoreactivity

Immunoreactivity for GABA in both V2 and MT was similar in both laminar and subcellular distribution to GABA immunoreactivity in V1 (Kelly et al. 2019). Anti-GABA label was visible primarily in cell bodies. Labeled neurons varied in size and shape (Figs. 1, 2) and were present in all cortical layers (Fig. 3), including layer 1. In both cortical areas, GABA-labeled neurons were most prevalent in terms of absolute density in layers 2 (V2: 20.2×10^3 neurons per mm^3; MT: 48.1×10^3 neurons per mm^3), 3A (V2: 26.8×10^3 neurons per mm^3; MT: 33.4×10^3 neurons per mm^3), and 4 (V2: 29.8×10^3 neurons per mm^3; MT: 34.4×10^3 neurons per mm^3). These are also the layers with the highest total neuronal density (Fig. 3; Tables 1, 2). Overall, GABA-labeled neurons were more prevalent in MT than in V2, both

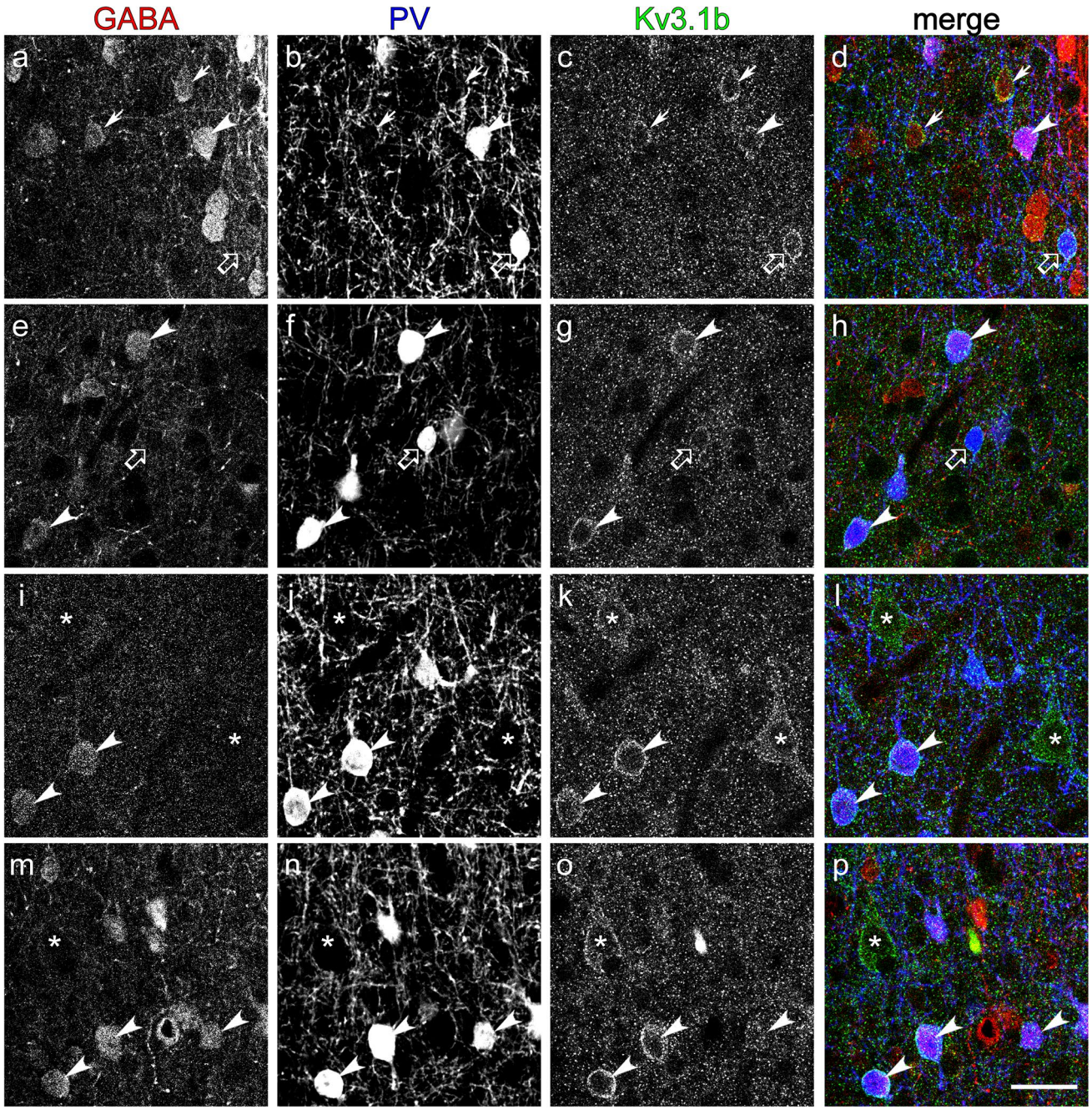

Fig. 1 Patterns of co-immunoreactivity of GABA, PV, and Kv3.1b in V2. Confocal micrographs from layers 2 (**a**–**d**), 3B (**e**–**h**), and 3C/4 (**i**–**p**) reveal that neurons expressed various combinations of GABA (**a**, **e**, **i**, **m**), PV (**b**, **f**, **j**, **n**), and Kv3.1b (**c**, **g**, **k**, **o**). Farthest right column shows an overlay of the GABA (red), PV (blue), and Kv3.1b (green) channels. Asterisks: layer 3C neurons immunoreactive only for Kv3.1b. Filled arrows: Kv3.1b+/GABA+/PV− neurons. Open arrows: Kv3.1b+/PV+/GABA− neurons. Arrowheads: Kv3.1b+/PV+/GABA+ neurons. Scale bar in **p** (refers to all panels): 25 µm

numerically and as a fraction of the total neuronal population. In each of layers 2–6, GABA+ neurons comprised between 10 and 17% of the total neuronal population in V2; the average proportion of GABA+ neurons relative to all neurons across all layers of V2 was 14%, slightly higher than the proportion measured in V1 (11%; Kelly et al. 2019) but considerably lower (by almost half) than previously reported for area 18 (25%; Hendry et al. 1987). In MT, the proportion of neurons that were GABAergic ranged from 20 to 25% in layers 2–6, comprising 25% of the population across all layers. This difference did not correspond to any obvious difference in quality of immunofluorescent label or counting

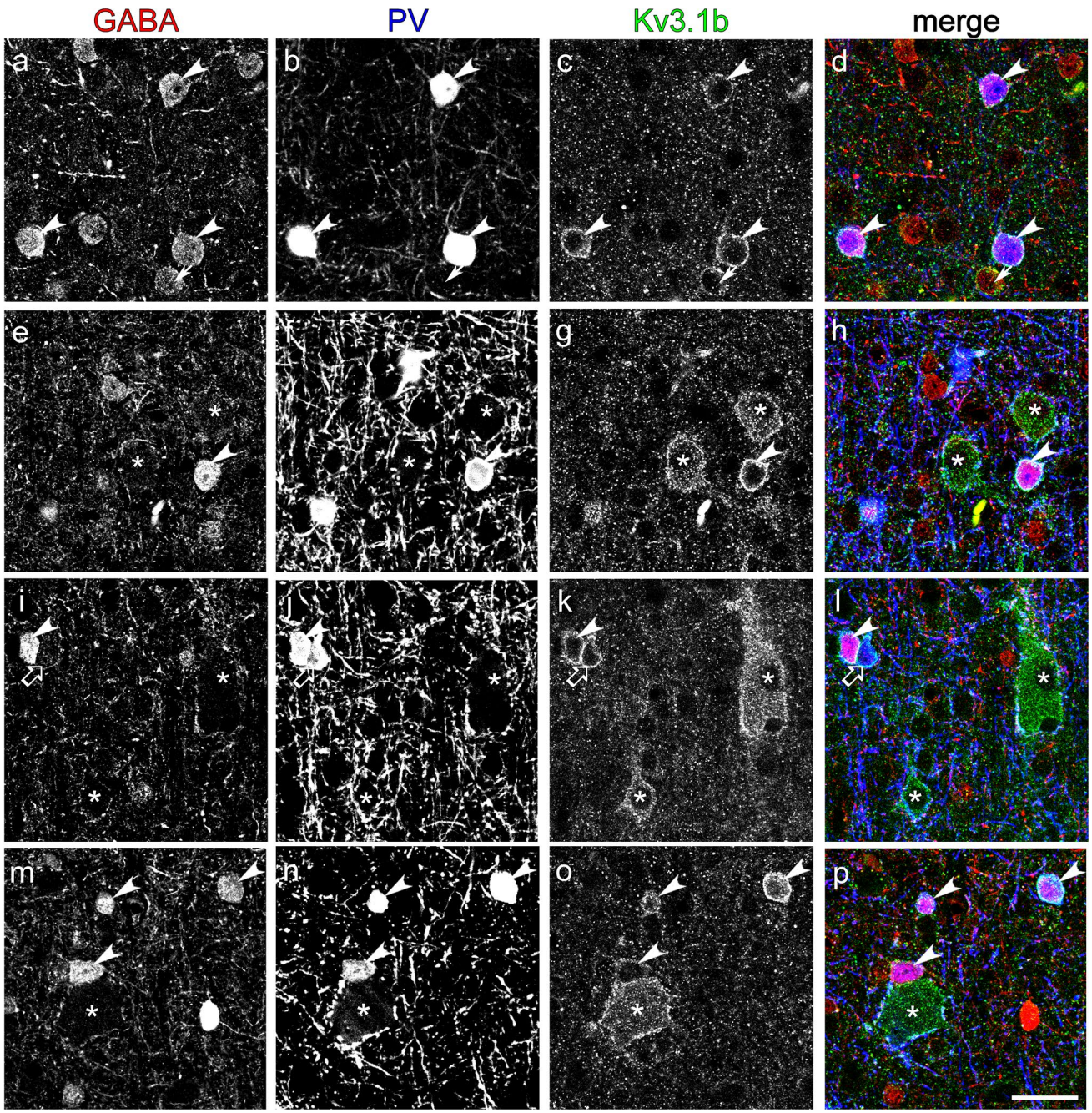

Fig. 2 Patterns of co-immunoreactivity of GABA, PV, and Kv3.1b in MT. Confocal micrographs from layers 2 (**a**–**d**), 3C (**e**–**l**), and 5 (**m**–**p**). Farthest right column shows an overlay of the GABA (red), PV (blue), and Kv3.1b (green) channels. Asterisks: neurons immunoreactive only for Kv3.1b. Filled arrows: Kv3.1b+/GABA+/PV− neurons. Open arrows: Kv3.1b+/PV+/GABA− neurons. Arrowheads: Kv3.1b+/PV+/GABA+ neurons. Scale bar in **p** (refers to all panels): 25 µm

criteria, nor did it appear to correspond to differences in either the extent of antibody penetration or sampling of regions beyond the range of antibody penetration. Anti-PV, rather than anti-GABA, typically limited the region available for sampling by having the most limited penetration into the tissue. The positions of counted GABA+ cells from all V2 samples relative to the depth into the corresponding tissue sections are shown in Supplementary Fig. 2; there does not appear to be a falloff in GABA+ cell detection with increasing distance from the cut tissue surface that could account for the lower GABA+ cell densities observed in V2 compared with MT. As in other areas (Hendry et al. 1987; Beaulieu et al. 1992; Kelly et al. 2019), the density of GABA+ neurons relative to the total neuronal population

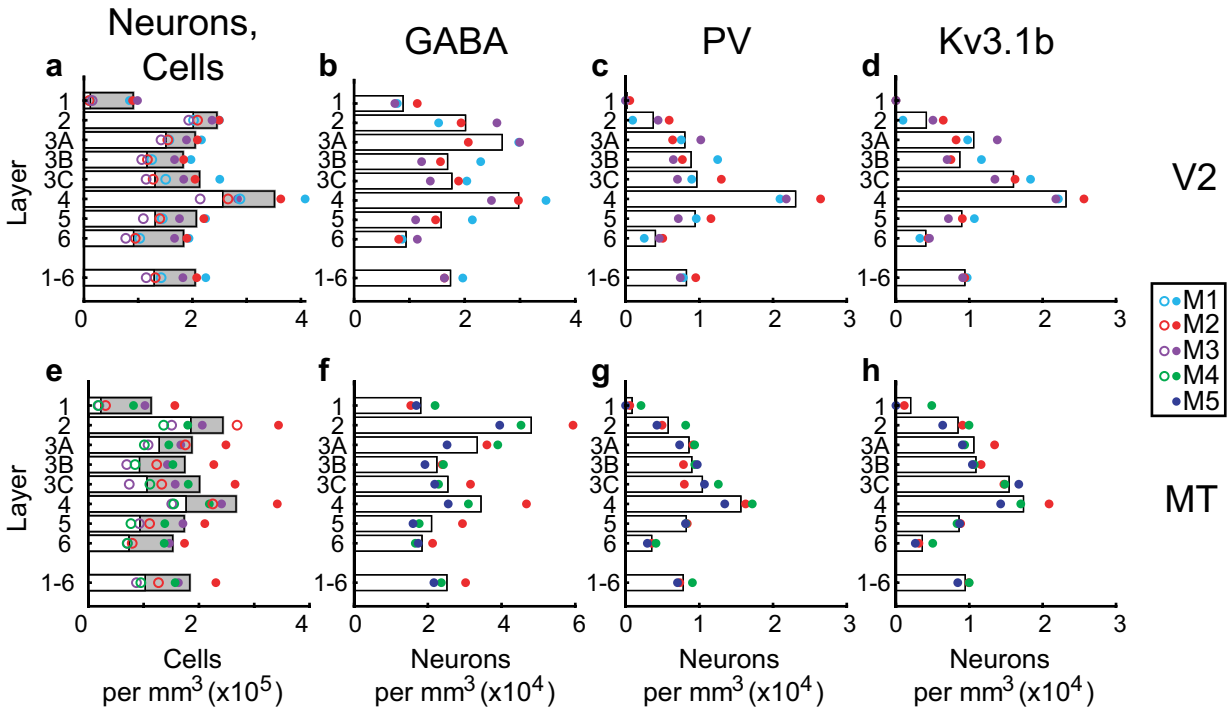

Fig. 3 Density distributions of cell populations in V2 (**a**–**d**) and MT (**e**–**h**). **a**, **e**: Density per mm^3 of DAPI-labeled cells (filled gray bars, filled points) and neurons (overlaid white bars, open points) in each layer. **b**, **f**: Density of GABA+ neurons, regardless of co-immunoreactivity for PV or Kv3.1b, in each layer. **c**, **g** Density of PV+ neurons in each layer. **d**, **h** Density of Kv3.1b+ neurons in each layer. Data points represent average densities from individual animals (M1–M5), with colors indicating the same animal across data sets. Bars represent means across animals

was markedly higher in layer 1 (V2: 74%; MT: 89%) than in other layers.

PV immunoreactivity

PV+ neurons were also present in all layers (Fig. 3), although they were sparse in layer 1 (V2: 0.2×10^3 neurons per mm^3; MT: 1.1×10^3 neurons per mm^3). The highest density of PV+ neurons was in layer 4 (V2: 23.1×10^3 neurons per mm^3; MT: 15.6×10^3 neurons per mm^3), corresponding to 9% of all layer 4 neurons in each area. Density and relative prevalence of PV+ neurons increased throughout layers 1 through 4 and then decreased from layers 4 through 6 (Fig. 3). This divergence from the distribution of GABA+ neurons suggests that, as in V1, PV− types of GABAergic neurons [e.g. calbindin (CB)- and calretinin (CR)-expressing types] are relatively more frequent in the supragranular layers in V2 and MT, consistent with previous reports (Kondo et al. 1994; DeFelipe et al. 1999).

Co-expression of GABA and PV

Although the density of GABA+ neurons was higher than the density of PV+ neurons in all layers, this difference was largest in the most superficial layers of V2 and MT. In layer 4 of V2 (but not MT), the densities of GABA+ and PV+ neurons were quite similar, and in layer 4 of both areas, the proportion of GABA+ neurons that were PV+ was higher (V2: 69%; MT: 44%) than in other layers (Fig. 4). In general, the laminar pattern of co-expression of GABA and PV in V2 was highly reminiscent of the pattern observed in V1. In V1, the proportions of GABA+ neurons co-expressing PV in layer 1 and in the upper third of layer 2/3 were 0% and 24%, respectively (Kelly et al. 2019); in V2, the proportions of GABA+ neurons that were PV+ in layers 1 (2%) and 2-3A (23%) were strikingly similar. The rate of PV co-immunoreactivity of GABA+ neurons in layer 4 of V2 (69%) was similar to the rate observed in layer 4A of V1 (73%); in layer 4C of V1, 79% of GABA+ neurons were PV+ (Kelly et al. 2019). Across all cortical layers of V2, 42% of GABA+ neurons were PV+, which is a bit lower than the 52% of GABA+ neurons that were PV+ in V1. In MT, the relative distribution of PV+ neurons was largely similar to those observed in both V1 and V2, but the fraction of GABAergic neurons that were PV+ was considerably lower (29%); that is, there were overall more MT neurons labeled for GABA but not PV.

Although most PV+ neurons were GABA+ (V2: 88%, MT: 92%), there were also PV+ neurons with no discernable GABA immunoreactivity (Figs. 1, 2, open arrows). This

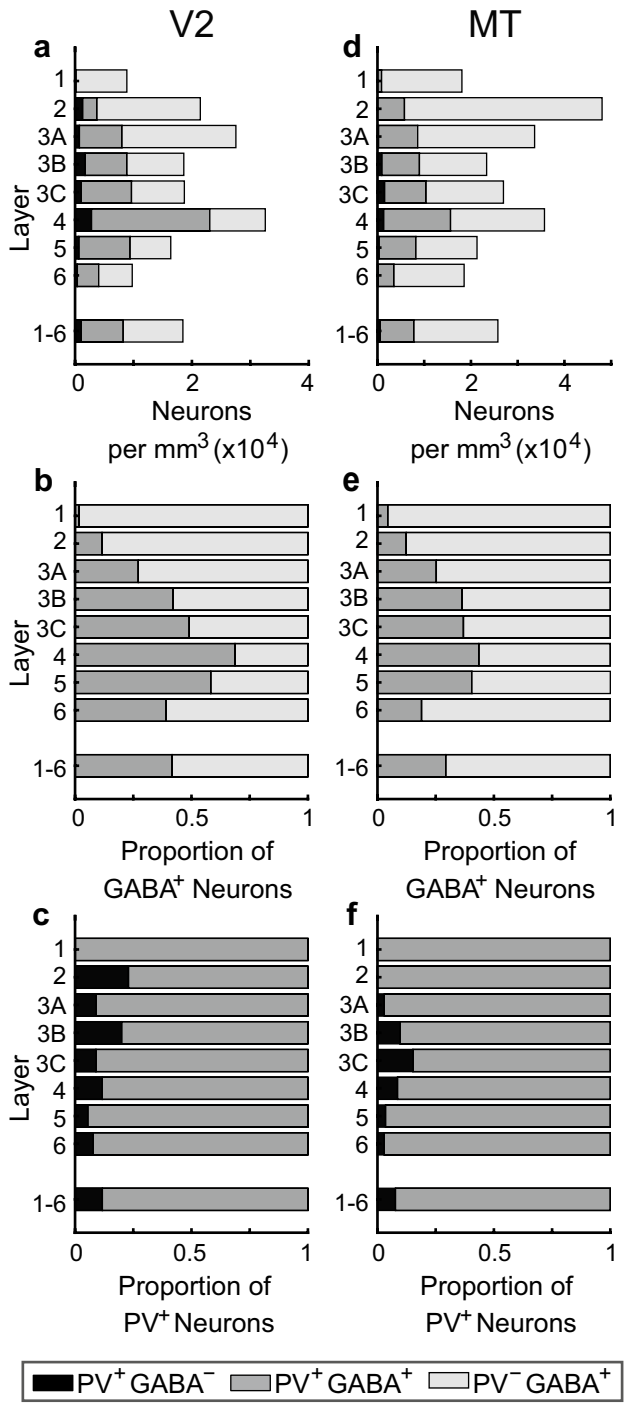

Fig. 4 Co-expression of PV and GABA in V2 (**a**–**c**) and MT (**d**–**f**). **a**, **d** Density per mm^3 of neurons immunoreactive for GABA (light gray), PV (black), or both (dark gray) in each layer. Bars are stacked. **b**, **e** Proportion of all GABA+ neurons in each layer that were (dark gray) or were not (light gray) also PV+. **c**, **f** Proportion of all PV+ neurons in each layer that were (dark gray) or were not (black) also GABA+. To facilitate comparison with V1, conventions match those of Fig. 5b–d of Kelly et al. (2019)

compares with 96% of PV+ neurons that were GABA+ in V1 (Kelly et al. 2019).

Co-expression of Kv3.1b with GABA and PV

The subcellular localization of Kv3.1b immunoreactivity was similar to that observed previously (Weiser et al. 1995; Du et al. 1996; Härtig et al. 1999; Hernández-Pineda et al. 1999; Kelly et al. 2019). Kv3.1b staining was primarily found in the cell membrane surrounding the somata of neurons classified as Kv3.1b+ and sometimes extended into the cell membrane associated with the proximal dendrites (Figs. 1, 2). As in V1, the distribution of Kv3.1b+ neurons (Fig. 3) was generally similar to the distribution of PV+ neurons in both V2 and MT, which reflects that Kv3.1b and PV are frequently co-expressed within the same neurons. The highest absolute densities of Kv3.1b+ neurons were in layer 4 (V2: 23.2×10^3 neurons per mm^3; MT: 17.4×10^3 neurons per mm^3), where they comprised 10% of all neurons. However, although the absolute densities of Kv3.1b+ neurons were lower in layer 3C (V2: 16.0×10^3 neurons per mm^3; MT: 15.4×10^3 neurons per mm^3), these densities corresponded to 13% and 15% of all neurons in layer 3C of V2 and MT, respectively, and exceeded the densities of PV+ neurons in the same layer (V2: 9.7×10^3 neurons per mm^3; MT: 10.4×10^3 neurons per mm^3).

Kv3.1b+/GABA−/PV− neurons

Averaged across the full cortical depth in each area, 71% of all Kv3.1b+ neurons were both GABA+ and PV+. However, as in V1, substantial subpopulations of Kv3.1b+ neurons in V2 and MT were neither PV+ nor GABA+, with average densities across all layers of 1.5×10^3 neurons per mm^3 in V2 and 1.6×10^3 neurons per mm^3 in MT. These densities correspond to approximately 1% and 2% of all neurons in V2 and MT, respectively, but 16% of all Kv3.1b+ neurons in both areas. As in V1, Kv3.1b+/GABA−/PV− neurons were highly compartmentalized within V2 and MT. In both areas, the highest densities of these neurons were found in layer 3C (V2: 6.6×10^3 neurons per mm^3; MT: 5.5×10^3 neurons per mm^3), where they comprised approximately 5% of the total neuronal population. About half of all observed Kv3.1b+/GABA−/PV− neurons were located in this layer (V2: 58 out of 96 neurons; MT: 71 out of 140 neurons), which spanned only 14% of the total cortical depth. In V2 and MT, respectively, 41% and 36% of all Kv3.1b+ neurons in layer 3C were neither GABA+ nor PV+.

Although the morphology of Kv3.1b+/GABA−/PV− neurons could not always be identified, many had clear pyramidal morphology, and some were particularly large pyramidal neurons located in layer 3C (Figs. 1, 2). Occasionally, and especially in the largest neurons, Kv3.1b label appeared diffusely

present in the perikaryal cytoplasm, but it was enhanced in the cell membrane. Many Kv3.1b+/GABA− pyramidal neurons were surrounded by a plexus of PV+ processes, presumably including the axon terminals of basket cells, similar to the pattern of PV immunoreactivity surrounding many Kv3.1b+/GABA−/PV− neurons in V1 (Kelly et al. 2019). As for V1 neurons, Kv3.1b signal was present adjacent to the PV-immunoreactive plexus, but there was also more continuous membrane immunoreactivity for Kv3.1b visible in the regions between punctate PV staining. We also observed several examples of very large layer 5 pyramidal neurons (Fig. 2m–p, asterisks) that were Kv3.1b+/GABA−/PV−; more examples were observed in MT than in V2. Similar large layer 5 Kv3.1b+ pyramidal neurons, as well as weakly Kv3.1b+ pyramidal neurons in the lower portion of layer 3, have been observed in multiple brain areas (Ichinohe et al. 2004).

Kv3.1b and inhibitory subpopulations

In V1, PV and GABA were expressed with near perfect correspondence in the Kv3.1b+ subpopulation. That is, PV expression almost completely and exclusively identified the Kv3.1b+/GABA+ subpopulation, and absence of PV in Kv3.1b+ neurons indicated an absence of GABA; 96% of Kv3.1b+/PV+ neurons in V1 were also GABA+, and 99% of Kv3.1b+/GABA+ neurons were also PV+ (Kelly et al. 2019). This was largely the case in layers 4–6 of V2 and MT. Of Kv3.1b+/PV+ neurons in layers 4 through 6, 93% (in V2) and 96% (in MT) were also GABA+. Of Kv3.1b+/GABA+ neurons in these layers, 99% (in V2) and 98% (in MT) were also PV+. In contrast, in layers 2 through 3C, 87% (V2) and 92% (MT) of Kv3.1b+/PV+ neurons were GABA+, and 86% (V2) and 83% (MT) of Kv3.1b/GABA+ neurons were PV+.

Kv3.1b+/GABA+/PV− neurons were observed in V1 (Kelly et al. 2019) and were suspected to be the Kv3.1b+/CB+ neurons observed by Constantinople et al. (2009), but they were very infrequently present. In V2, however, 11% of Kv3.1b+ neurons in layer 2 and 25% of Kv3.1b+ neurons in layer 3A were GABA+ but PV− (Fig. 5). In MT, 35% of Kv3.1b+ neurons in layer 2 and 24% of Kv3.1b+ neurons in layer 3A were GABA+ but PV−. The laminar distribution of Kv3.1b+/GABA+/PV− neurons is consistent with the hypothesis that they include CB+ neurons, which are most populous in the most superficial layers (Kondo et al. 1994; DeFelipe et al. 1999).

Discussion

The current studies extend a quantitative anatomical examination, in visual cortex, of what may constitute a molecularly and functionally distinct class of excitatory neuron. The

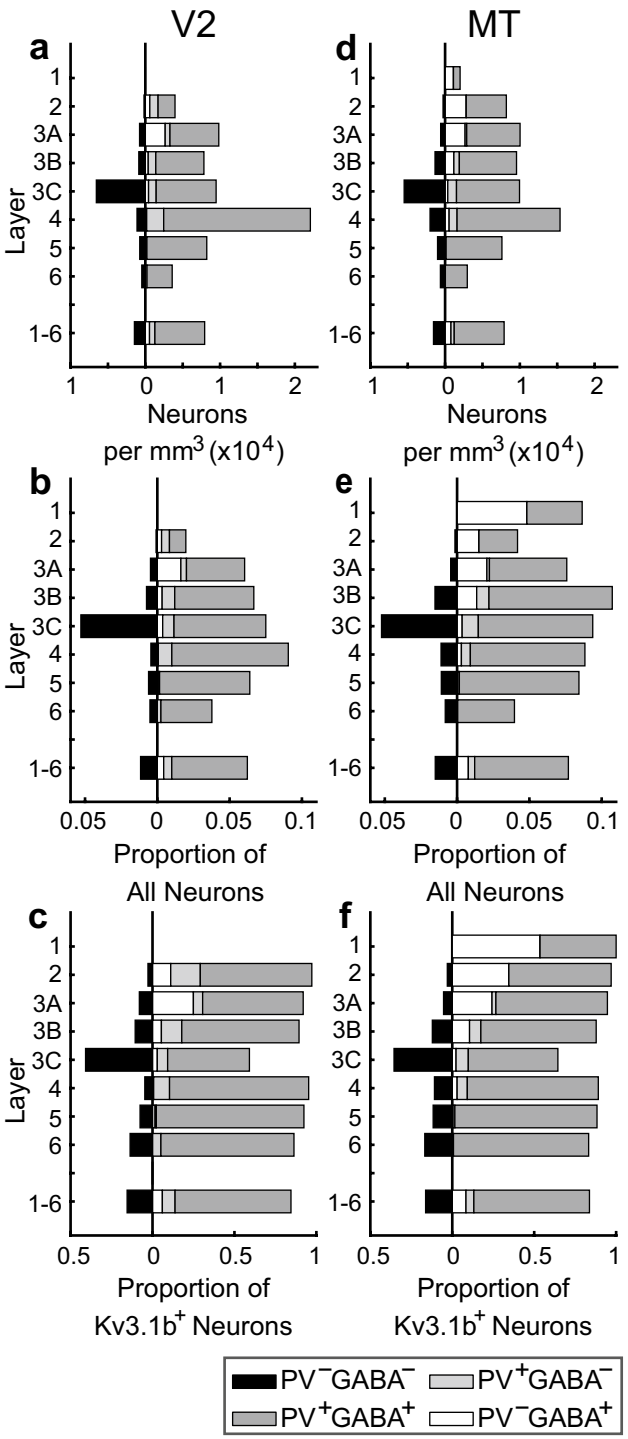

Fig. 5 Laminar distributions of Kv3.1b+ subpopulations in V2 (**a**–**c**) and MT (**d**–**f**). **a**, **d** Density per mm^3 of Kv3.1b+/GABA−/PV− neurons (black; left of vertical); Kv3.1b+/GABA+/PV− (white); Kv3.1b+/GABA−/PV+ (light gray); and Kv3.1b+/GABA+/PV+ (dark gray) neurons in each layer. **b**, **e** Frequency of cell types as in **a**, **d** as a fraction of the total neuronal population in the same layer. **c**, **f** Frequency of cell types as in **a**, **d** as a fraction of all Kv3.1b+ neurons at the same cortical depth. To facilitate comparison with V1, conventions match those of Fig. 6b–d of Kelly et al. (2019)

neuronal population of primary interest expresses the potassium channel subunit Kv3.1b but neither PV nor GABA, indicating that these neurons likely have narrow spike widths and may exhibit a fast-spiking phenotype characteristic of PV-expressing inhibitory interneurons. Kv3.1b+/GABA−/PV− neurons showed laminar specificity in both V2 and MT; they were most frequently observed in layer 3C, where they comprised 41% (in V2) and 36% (in MT) of all Kv3.1b + neurons. This laminar specificity is reminiscent of the pattern recently observed in V1 (Kelly et al. 2019), suggesting a common circuit organization for this particular subpopulation across cortical areas.

PV and GABA expression in V2 and MT

PV+ neurons

The average density of PV+ neurons across layers 1–6 of V2 was 8.3×10^3 neurons per mm^3, approximately 6% of the estimated density of neurons of all types (Fig. 3). This is well matched to the estimated fraction of neurons that were PV+ in V1 (6–7%; Kelly et al. 2019); it was previously observed that the ratios of PV+ neurons relative to all Nissl-stained cells were similar between V1 and V2 (Kondo et al. 1994). Kondo et al. (1994) also observed that the laminar distribution of PV+ neurons was similar across cortical areas, with PV+ neurons present across layers 2–6 but densest in layer 4. Similarly, the density of PV+ neurons in the current study was highest in layer 4 (V2: 23.1×10^3 neurons per mm^3; MT: 15.6×10^3 neurons per mm^3), accounting for 9% of all layer 4 neurons. In general, laminar distributions of PV+ neurons appear to differ very little across cortical areas; PV− interneurons predominate in the upper layers, whereas PV+ neurons are most abundant in the middle layers (Van Brederode et al 1990; Kondo et al. 1994; DeFelipe et al. 1999; Kelly et al. 2019), even in agranular prefrontal cortical areas (Conde et al. 1994; Gabbott and Bacon 1996). In visual areas V1 (Kelly et al. 2019), V2, and MT and in prefrontal cortical areas (Gabbott and Bacon 1996), PV+ neurons consistently account for 5–7% of the total neuronal population.

A previous investigation found higher PV+ neuronal densities in layers 3 and 5 than in layer 4 of MT (Dhar et al. 2001), which conflicts with our results and with previous results in other areas (Van Brederode et al. 1990; Kondo et al. 1994; Kelly et al. 2019). We also observed an average PV+ density about double that measured by Dhar et al. (2001). In layers 2/3 of V2, we found that PV+ neurons accounted for about 6% of the total neuronal population, which is similar to a previous report (5%: Sherwood et al. 2007), although the PV+ density reported in the previous study (14.4×10^3 neurons per mm^3) was 1.8 times our estimate (8.1×10^3 neurons per mm^3).

GABA+ neurons

The laminar distribution of GABA+ neurons in V2 and MT (Fig. 3) was consistent with previous studies of V1 and V2 (Hendry et al. 1987; Beaulieu et al. 1992; Kelly et al. 2019). There are no direct reports of the numerical density of GABAergic neurons in the macaque monkey either overall or within individual layers in V2 or MT. Because the calcium-binding proteins PV, CB, and CR are considered to identify largely non-overlapping subpopulations of GABAergic interneurons (Hendry et al. 1989; Condé et al. 1994; Meskenaite 1997; Vickers et al. 1993), measuring their density in combination may approximate the overall GABAergic population. In layer 2/3 of V2 of *Macaca maura* (Sherwood et al. 2007), the combined density of PV+, CB+, and CR+ neurons in layers 2/3 of V2 (52.5×10^3 neurons per mm^3) was 2.6 times the density of GABA+ neurons measured in the current study across layers 2–3C (20.0×10^3 neurons per mm^3). The previous density estimate could be artificially high due to some overlap in calcium-binding protein immunoreactivity, the inclusion of some non-GABAergic neurons in the CB+ population (Van Brederode et al. 1990; Disney and Aoki 2008), and shrinkage in the x and y dimensions that was not corrected for; nevertheless, this is a substantial difference.

The total density of layer 2/3 neurons in V2 estimated in the Sherwood et al. (2007) study (299×10^3 neurons per mm^3) was about double our estimate (141×10^3 neurons per mm^3) such that the combined calcium-binding protein-labeled population corresponded to 18% of the total neuronal population, in contrast to the 14% of all neurons that were GABA+ in the current study. Hendry et al. (1987) measured an even higher fraction of the total neuronal population in V2 that were GABA+ (24–25%). Both Hendry et al. (1987) and Sherwood et al. (2007) measured the total neuronal population by identifying Nissl-stained nuclei, a strategy that often leads to substantially different estimates of the neuronal population compared to the use of NeuN (Gittins and Harrison 2004; Giannaris and Rosene 2012; Kelly and Hawken 2017). A study counting NeuN- and glutamic acid decarboxylase-immunoreactive neurons in rat somatosensory cortex (Meyer et al. 2011) also yielded a lower proportion of GABAergic neurons compared with previous studies (12% vs. 15–25%), a difference the authors attributed primarily to the use of large 3D counting volumes. In our previous study of V1 (Kelly et al. 2019), densities of GABA+ neurons were well matched to previously reported values (Hendry et al. 1987; Beaulieu et al. 1992); however, because our measurement of the total population yielded substantially higher density values, our estimate of the fraction of the population that was GABAergic was much lower (11% vs. 20%). The total neuronal density we measured in V1 was consistent with a previous stereological study using

3D counting volumes in NeuN-labeled tissue (Giannaris and Rosene 2012). In V1, nearly the entire PV+ population was classified as GABA+, arguing at least against a general (non-subtype-specific) detection failure for GABA; we concluded that the discrepancy in proportion of GABAergic neurons was most likely due to prior underestimates of the total neuronal population. Although Hendry et al. (1987) did not report GABA+ neuronal density values in V2 to which we can compare our results, a similar discrepancy in estimating the total neuronal population may underlie the difference in fraction of V2 neurons that were GABA+ between studies.

Compared with V1 and V2, we identified a higher density of GABA+ neurons in MT, corresponding to 25% of all neurons, using identical tissue processing and cell-counting protocols. This substantially exceeds the fraction of neurons that were GABA+ in V2 or V1 (Kelly et al. 2019). It is interesting to speculate about the potential consequences this might have for cortical processing in these areas, although measurements of cell densities alone are wholly insufficient to discriminate between various hypotheses. There may be differences between areas in the total strength of inhibition and/or of the balance between excitation and inhibition. Alternatively, individual excitatory neurons in MT might receive weaker inhibitory inputs from each of a larger number of GABAergic neurons.

PV and GABA co-expression

The density of GABA+ neurons exceeded the density of PV+ neurons in all layers of V2 and MT (Fig. 3), and this difference was greatest in the superficial layers, where many GABAergic neurons do not express PV (Van Brederode et al. 1990; Conde et al. 1994; Kondo et al. 1994; Gabbott and Bacon 1996; DeFelipe et al. 1999). The proportion of GABA+ neurons that were PV+ was highest in layer 4 (V2: 69%; MT: 44%). The similarity in the laminar pattern of PV and GABA co-immunoreactivity between V1 and V2 may indicate that the PV-expressing GABAergic interneurons have similar circuit roles in both areas. A few differences across areas are worth noting, however. First, the proportion of PV+ neurons that co-expressed GABA was lower in V2 (88%) compared to V1 (96%). This difference is not well explained by a general underestimation of GABA immunoreactivity in V2, because the overall proportion of GABA+ neurons that co-expressed PV was also lower in V2 (42%) compared to V1 (52%). The fraction of PV+ neurons co-expressing GABA was intermediate in MT (92%). While PV+/GABA− neurons were not observed in the infragranular layers in V1, in V2 they comprised a fairly similar fraction of the PV+ population across layers 2–6 (Fig. 4). Second, the relationship between PV and GABA expression in the Kv3.1b+ population was looser in V2 and MT than in V1, as discussed below. Third, the fraction of GABA+ neurons co-expressing PV was much lower in MT than in V1 and V2; that is, substantially more GABA+ neurons in MT were PV−. Whereas the PV+ population accounts for a similar fraction of the total neuronal population across areas, PV− types of GABA+ neurons vary more in prevalence, at least between these three visual areas.

Kv3.1b+/GABA+/PV− neurons in V2 and MT

In V1, we observed a nearly perfect correspondence between PV and GABA in Kv3.1b+ neurons (Kelly et al. 2019). In V2, in contrast, 90% of Kv3.1b+/PV+ neurons were GABA+, and 92% of Kv3.1b+/GABA+ neurons were PV+ (Fig. 5). In our previous study of V1, Kv3.1b+/GABA+/PV− neurons were rarely observed but were suspected to correspond to the Kv3.1b+/CB+ neurons identified by Constantinople et al. (2009). In both V2 and MT, these neurons appeared more frequently. Across layers, 6% and 8% of Kv3.1b+ neurons in V2 and MT, respectively, were GABA+ and PV−, compared to 1% of Kv3.1b+ neurons in V1. This neuronal subpopulation was most frequently observed in layers 2–3B, where CB+ neurons are more prevalent (Kondo et al. 1994; DeFelipe et al. 1999). Therefore, the fast-spiking inhibitory interneuron population in macaque V2 and MT could be expected to include CB+ neurons rather than exclusively PV+ neurons. Compared with V1, V2 also had more neurons that expressed PV and Kv3.1b but had no visible GABA immunoreactivity (Fig. 1, open arrows).

Kv3.1b+/GABA− neurons in V2 and MT

A majority of Kv3.1b+ neurons in layers 2 through 6 were both PV+ and GABA+. Relatively minor Kv3.1b+ populations were also immunoreactive for either PV or GABA but not both. As in V1, both V2 and MT also contained substantial subpopulations of Kv3.1b+ neurons that were neither GABA+ nor PV+ (Figs. 1, 2, asterisks). Across layers 1–6, 23% of Kv3.1b+ neurons in V2 and 21% of Kv3.1b+ neurons in MT were GABA−, and 16% of all Kv3.1b+ neurons in both areas were GABA− and PV−. Kv3.1b+/GABA−/PV− neurons were preferentially located in layer 3C (Fig. 5; Tables 3, 4), where 47% of Kv3.1b+ V2 neurons were GABA− and 41% were both GABA− and PV−. In layer 3C of MT, 43% of Kv3.1b+ neurons were GABA− and 36% were both GABA− and PV−.

The morphology of these neurons could not always be identified and was not systematically studied. However, Kv3.1b+/PV+/GABA− neurons often had small non-pyramidal cell bodies (Figs. 1, 2, open arrows), and so it is unclear whether they should be interpreted as excitatory neurons. Kv3.1b+/GABA−/PV− neurons were often clearly pyramidal neurons (Figs. 1, 2, asterisks). Kv3.1b+ pyramidal neurons were previously observed in layer 5 and

the lower part of layer 3 of multiple cortical areas, including V2, but were reportedly absent in MT (Ichinohe et al. 2004). In contrast, in the current study, there were many clear examples of Kv3.1b+ pyramidal neurons in MT (Fig. 2e–p, asterisks), with a similar prevalence and distribution to the corresponding subpopulation in V2. In both areas, these pyramidal neurons varied in size—compare two neighboring examples in layer 3C of MT in Fig. 2i–l (asterisks)—but included the largest pyramidal neurons in layer 3C. Consistent with previous observations (Elston and Rosa 1997), these large layer 3C pyramidal neurons were larger in MT (Fig. 2e–l) than in V2 (Fig. 1i–p).

Compartmentalization of Kv3.1b+/GABA−/PV− neurons in V1, V2, and MT

In V1 (Kelly et al. 2019), Kv3.1b+/GABA−/PV− neurons were predominantly located in layers 4B and 4Cα, using the nomenclature scheme of Brodmann (1909) and Lund (1973). This layer continues across the V1/V2 border as the lowermost portion of layer 3, such that Brodmann's (1909) layer 4B is more aptly considered a subdivision of layer 3 (Balaram and Kaas 2014; Balaram et al. 2014), as it is designated in other nomenclature schemes (e.g. Hässler 1966; Spatz et al. 1970). The relative prevalence of Kv3.1b+/GABA−/PV− neurons in Brodmann's layer 4B in V1 (Kelly et al. 2019) and in layer 3C in V2 and MT constitutes an additional commonality between these likely homologous cytoarchitectonic compartments (Casagrande and Kaas 1994; Balaram et al. 2014) and suggests that this neuronal subpopulation may have a specialized function in the cortical circuit that is common across areas.

Limitations and future directions

Laminar boundaries were delimited as single horizontal lines through each image series, relying mainly on visual identification of changes in cell composition and density (see "Materials and methods"). This strategy cannot precisely capture the transitions between layers, which are not always perfectly parallel to each other and do not always show a stark difference in density. The transition from layer 6 to the white matter can be particularly difficult to identify, and across studies may be differently demarcated. The average cell density measurements from each layer (Tables 1, 2) suggest that at least between our measurements of total neuronal density (using NeuN) and of subpopulations (using GABA, PV, and Kv3.1b) the corresponding laminar regions have been consistently identified. Nevertheless, density estimates for each layer are likely contaminated to some extent by partial inclusion of neighboring layers and, therefore, may underrepresent differences between layers. Computing densities of different cell types using only the middle third of each layer (Supplementary Tables 1–4) does suggest some contamination of this kind, but the overall patterns described—including the higher prevalence of Kv3.1b+/GABA−/PV− neurons in layer 3C—are unchanged in this restricted analysis. It should be noted that reducing the regions analyzed in this way makes the estimates more vulnerable to error particularly when cell counts are small.

The distribution of the Kv3.1b+/GABA−/PV− population in V1—nearly exclusive to layers 4Cα and 4B, in addition to the MT-projecting Meynert cells at the upper border of layer 6—was consistent not only with a layer-specific organization but also with the alternative possibility of an association with the magnocellular (M) pathway and dorsal visual pathways (Kelly et al. 2019). This is because layer 4Cα receives direct geniculate input specifically from the M layers (Hubel and Wiesel 1972; Hendrickson et al. 1978); layer 4B neurons receive feedforward input primarily from layer 4Cα spiny stellate neurons (Yoshioka et al. 1994); both the Meynert cells and a subset of layer 4B neurons project directly to MT (Lund et al. 1975; Fries and Distel 1983; Fries et al. 1985; Hof et al. 1996; Nhan and Callaway 2012); and some neurons in layer 4B project to the thick stripes of V2 (Livingstone and Hubel 1987; Federer et al. 2009), which are a source of MT afferents (Shipp and Zeki 1985, 1995). This association leads to the hypothesis that Kv3.1b+ excitatory neurons might be primarily located in other cortical regions linked to the M pathway or dorsal stream. For example, they might be more frequent in area MT compared to V4, and they might be preferentially located in the cytochrome oxidase (CO)-rich thick stripes in V2 compared to other CO-defined compartments. Kv3.1b+ pyramidal/non-GABAergic neurons have been identified in multiple cortical areas, including non-visual areas (Härtig et al. 1999; Ichinohe et al. 2004; Soares et al. 2017), so this class of cells cannot be exclusive to the visual M pathway or the dorsal stream. However, the results of the current study are insufficient to rule out the possibility of a pathway-specific bias in the distribution of Kv3.1b+/GABA−/PV− neurons in visual cortex. The CO stripe compartments of the V2 samples used in the current study were unknown and may not have included all stripe regions or represented those regions equally. Notably, however, Kv3.1b+/GABA−/PV− layer 3C neurons were observed in all image series sampled from V2, and it is unlikely that they all coincidentally represented the thick stripes. It is, therefore, unlikely that Kv3.1b+/GABA−/PV− neurons are exclusive to the thick stripes, although examination of tangential sections from layer 3C would be useful to determine whether their distribution is biased toward the thick stripes. A direct comparison of the laminar distribution in MT with ventral stream-associated visual areas (e.g. V4), or of visual areas with non-visual cortical areas, would also be interesting in future studies.

The localization of Kv3.1b+/GABA−/PV− neurons in layer 3C suggests that they are likely to include neurons that make feedforward connections with other cortical areas. Layer 3C of V2 includes projecting neurons with a variety of cortical targets, including V4, MT, and the contralateral hemisphere (Glickstein and Whitteridge 1976; Wong-Riley 1974; Lund et al. 1975, 1981; Rockland and Pandya 1979; Kennedy et al. 1986; Shipp and Zeki 1989; Zeki and Shipp 1989). Furthermore, many Kv3.1b-expressing excitatory neurons we have identified in V1 (Kelly et al. 2019) and V2 and MT (current study) are situated to potentially receive direct feedforward excitatory input from other Kv3.1b-expressing neurons. In future experiments, it would be interesting to combine tracing techniques with identification of Kv3.1b expression to establish whether Kv3.1b+ pyramidal neurons are projecting neurons with specific downstream targets, and whether they are preferentially connected in a feedforward network.

Summary

In this study, the pattern of co-expression of Kv3.1b, PV, and GABA was evaluated in the extrastriate visual cortical areas V2 and MT. As expected, many neurons that expressed Kv3.1b also expressed both PV and GABA. However, like in V1, both V2 and MT contained neurons that were Kv3.1b+ but PV− and GABA−, and these were arranged with laminar specificity, with the highest frequency in layer 3C. In layer 3C of both areas, Kv3.1b+/GABA−/PV− neurons accounted for 5% of the total neuronal population and 36–41% of all Kv3.1b+ neurons. This is reminiscent of prior observations in V1 (Kelly et al. 2019) and suggests a similar circuit role for this particular neuronal subpopulation across multiple cortical areas. There were more neurons in V2 and MT that were Kv3.1b+ and GABA+ but PV− compared to in V1, and there was a greater dissociation between PV and GABA expression, even within the Kv3.1b+ population. Whereas PV+ neurons accounted for a similar fraction of the neuronal population across areas, GABA+ neurons accounted for a much higher fraction of the population in MT, an effect driven largely by an increase in the density of GABA+/Kv3.1b−/PV− neurons in MT.

Acknowledgements This work was supported by the National Institutes of Health, Grant numbers EY17945; P30EY013079; T32EY007136; and R01 EY022428 (to J. Anthony Movshon and Eero Simoncelli).

Compliance with ethical standards

Ethical approval All applicable international, national, and/or institutional guidelines for the care and use of animals were followed. All procedures performed in studies involving animals were in accordance with the ethical standards of the institution or practice at which the studies were conducted.

References

Balaram P, Kaas JH (2014) Towards a unified scheme of cortical lamination for primary visual cortex across primates: insights from NeuN and VGLUT2 immunoreactivity. Front Neuroanat 8:81

Balaram P, Young NA, Kaas JH (2014) Histological features of layers and sublayers in cortical visual areas V1 and V2 of chimpanzees, macaque monkeys, and humans. Eye Brain 6:5–18

Beaulieu C, Kisvarday Z, Somogyi P, Cynader M, Cowey A (1992) Quantitative distribution of GABA-immunopositive and -immunonegative neurons and synapses in the monkey striate cortex (area 17). Cereb Cortex 2:295–309

Brodmann K (1909) Localisation in the cerebral cortex. (Garey LJ, trans) Smith-Gordon, London

Casagrande VA, Kaas JH (1994) The afferent, intrinsic, and efferent connections of primary visual cortex in primates. In: Peters A, Rockland K (eds) Cerebral cortex, vol. 10: primary visual cortex of primates. Plenum Press, New York, pp 201–259

Cauli B, Audinat E, Lambolez B, Angulo MC, Ropert N, Tsuzuki K, Hestrin S, Rossier J (1997) Molecular and physiological diversity of cortical nonpyramidal cells. J Neurosci 17:3894–3906

Chow A, Erisir A, Nadal MS, Ozaita A, Lau D, Welker E, Rudy B (1999) K+ channel expression distinguishes subpopulations of parvalbumin- and somatostatin-containing neocortical interneurons. J Neurosci 19:9332–9345

Collins CE (2011) Variability in neuron densities across the cortical sheet in primates. Brain Behav Evol 78:37–50

Collins CE, Airey DC, Young NA, Leitch DB, Kaas JH (2010) Neuron densities vary across and within cortical areas in primates. Proc Natl Acad Sci 107:15927–15932

Condé F, Lund JS, Jacobowitz DM, Baimbridge KG, Lewis DA (1994) Local circuit neurons immunoreactive for calretinin, calbindin D-28k or parvalbumin in monkey prefrontal cortex: distribution and morphology. J Comp Neurol 341:95–116

Constantinople CM, Disney AA, Maffie J, Rudy B, Hawken MJ (2009) Quantitative analysis of neurons with Kv3 potassium channel subunits, Kv3.1b and Kv3.2, in macaque primary visual cortex. J Comp Neurol 516:291–311

Coppola JJ, Disney AA (2018) Most calbindin-immunoreactive neurons, but few calretinin-immunoreactive neurons, express the m1 acetylcholine receptor in the middle temporal visual area of the macaque monkey. Brain Behav 8:e01071

DeFelipe J, Alonso-Nanclares L, Arellano JI (2002) Microstructure of the neocortex: comparative aspects. J Neurocytol 31:299–316

DeFelipe J, González-Albo MC, Del Río MR, Elston GN (1999) Distribution and patterns of connectivity of interneurons containing calbindin, calretinin, and parvalbumin in visual areas of the occipital and temporal lobes of the macaque monkey. J Comp Neurol 412:515–526

Desimone R, Ungerleider LG (1986) Multiple visual areas in the caudal superior temporal sulcus of the macaque. J Comp Neurol 248:164–189

Dhar P, Mehra RD, Sidharthan V, Sharma K (2001) Parvalbumin and calbindin D-28K immunoreactive neurons in area MT of rhesus monkey. Exp Brain Res 137:141–149

Disney AA, Aoki C (2008) Muscarinic acetylcholine receptors in macaque V1 are most frequently expressed by parvalbumin-immunoreactive neurons. J Comp Neurol 507:1748–1762

Disney AA, Reynolds JH (2014) Expression of m1-type muscarinic acetylcholine receptors by parvalbumin-immunoreactive neurons in the primary visual cortex: a comparative study of rat, guinea pig, ferret, macaque, and human. J Comp Neurol 522:986–1003

Du J, Zhang L, Weiser M, Rudy B, McBain CJ (1996) Developmental expression and functional characterization of the

potassium-channel subunit Kv3.1b in parvalbumin-containing interneurons of the rat hippocampus. J Neurosci 16:506–518
Elston GN, Rosa MGP (1997) The occipitoparietal pathway of the macaque monkey: comparison of pyramidal cell morphology in layer III of functionally related cortical visual areas. Cereb Cortex 7:432–452
Erisir A, Lau D, Rudy B, Leonard CS (1999) Function of specific K^+ channels in sustained high-frequency firing of fast-spiking neocortical interneurons. J Neurophysiol 82:2476–2489
Federer F, Ichida JM, Jeffs J, Schiessl I, McLoughlin N, Angelucci A (2009) Four projection streams from primate V1 to the cytochrome oxidase stripes of V2. J Neurosci 29:15455–15471
Fries W, Distel H (1983) Large layer VI neurons of monkey striate cortex (Meynert cells) project to the superior colliculus. Proc R Soc Lond B 219:53–59
Fries W, Keizer K, Kuypers HG (1985) Large layer VI cells in macaque striate cortex (Meynert cells) project to both superior colliculus and prestriate visual area V5. Exp Brain Res 58:613–616
Gabbott PL, Bacon SJ (1996) Local circuit neurons in the medial prefrontal cortex (areas 24a, b, c, 25 and 32) in the monkey: II. Quantitative areal and laminar distributions. J Comp Neurol 364:609–636
García-Marín V, Ahmed TH, Afzal YC, Hawken MJ (2013) Distribution of the vesicular glutamate transporter 2 (vGluT2) in the primary visual cortex of the macaque and human. J Comp Neurol 521:130–151
Giannaris EL, Rosene DL (2012) A stereological study of the numbers of neurons and glia in the primary visual cortex across the lifespan of male and female rhesus monkeys. J Comp Neurol 520:3492–3508
Gittins R, Harrison PJ (2004) Neuronal density, size and shape in the human anterior cingulate cortex: a comparison of Nissl and NeuN staining. Brain Res Bull 63:155–160
Glickstein M, Whitteridge D (1976) Degeneration of layer III pyramidal cells in area 18 following destruction of callosal input. Brain Res 104:148–151
Goris RLT, Simoncelli EP, Movshon JA (2015) Origin and function of tuning diversity in macaque visual cortex. Neuron 88:819–831
Härtig W, Derouiche A, Welt K, Brauer K, Grosche J, Mäder M, Reichenbach A, Brückner G (1999) Cortical neurons immunoreactive for the potassium channel Kv3.1b subunit are predominantly surrounded by perineuronal nets presumed as a buffering system for cations. Brain Res 842:15–29
Hässler R (1966) Comparative anatomy of the central visual systems in day and night-active primates. In: Hässler R, Stephan H (eds) Evolution of the forebrain. Thieme Verlag, Stuttgart, pp 419–434
Hendrickson AE, Wilson JR, Ogren MP (1978) The neuroanatomical organization of pathways between the dorsal lateral geniculate nucleus and visual cortex in Old World and New World primates. J Comp Neurol 182:123–136
Hendry SHC, Jones EG, Emson PC, Lawson DEM, Heizmann CW, Streit P (1989) Two classes of cortical GABA neurons defined by differential calcium binding protein immunoreactivities. Exp Brain Res 76:467–472
Hendry SHC, Schwark HD, Jones EG, Yan J (1987) Numbers and proportions of GABA-immunoreactive neurons in different areas of monkey cerebral cortex. J Neurosci 7:1503–1519
Hernández-Pineda R, Chow A, Amarillo Y, Moreno H, Saganich M, Vega-Saenz de Miera E, Hernández-Cruz A, Rudy B (1999) Kv3.1–Kv3.2 channels underlie a high-voltage-activating component of the delayed rectifier K^+ current in projecting neurons from the globus pallidus. J Neurophysiol 82:1512–1528
Hof PR, Morrison JH (1995) Neurofilament protein defines regional patterns of cortical organization in the macaque monkey visual system: a quantitative immunohistochemical analysis. J Comp Neurol 352:161–186
Hof PR, Sherwood CC (2005) Morphomolecular neuronal phenotypes in the neocortex reflect phylogenetic relationships among certain mammalian orders. Anat Rec A Discov Mol Cell Evol Biol 287A:1153–1163
Hof PR, Ungerleider LG, Webster MJ, Gattass R, Adams MM, Sailstad CA, Morrison JH (1996) Neurofilament protein is differentially distributed in subpopulations of corticocortical projection neurons in the macaque monkey visual pathways. J Comp Neurol 376:112–127
Horton JC (1984) Cytochrome oxidase patches: a new cytoarchitectonic feature of monkey visual cortex. Philos Trans R Soc Lond B 304:199–253
Howard V, Reid S, Baddeley A, Boyde A (1985) Unbiased estimation of particle density in the tandem scanning reflected light microscope. J Microsc 138:203–212
Hubel DH, Wiesel TN (1972) Laminar and columnar distribution of geniculo-cortical fibers in the macaque monkey. J Comp Neurol 146:421–450
Ichinohe N, Watakabe A, Miyashita T, Yamamori T, Hashikawa T, Rockland KS (2004) A voltage-gated potassium channel, Kv3.1b, is expressed by a subpopulation of large pyramidal neurons in layer 5 of the macaque monkey cortex. Neuroscience 129:179–185
Kawaguchi Y, Kubota Y (1993) Correlation of physiological subgroupings of nonpyramidal cells with parvalbumin- and $calbindin_{D28k}$-immunoreactive neurons in layer V of rat frontal cortex. J Neurophysiol 70:387–396
Kawaguchi Y, Kubota Y (1998) Neurochemical features and synaptic connections of large physiologically-identified GABAergic cells in the rat frontal cortex. Neurosci 85:677–701
Kelly JG, García-Marín V, Rudy B, Hawken MJ (2019) Densities and laminar distributions of Kv3.1b-, PV-, GABA-, and SMI-32-immunoreactive neurons in macaque area V1. Cereb Cortex 29:1921–1937
Kelly JG, Hawken MJ (2017) Quantification of neuronal density across cortical depth using automated 3D analysis of confocal image stacks. Brain Struct Funct 222:3333–3353
Kennedy H, Dehay C, Bullier J (1986) Organization of the callosal connections of visual areas V1 and V2 in the macaque monkey. J Comp Neurol 247:398–415
Kondo H, Hashikawa T, Tanaka K, Jones EG (1994) Neurochemical gradient along the monkey occipito-temporal cortical pathway. NeuroReport 5:613–616
Livingstone MS, Hubel DH (1987) Connections between layer 4B of area 17 and the thick cytochrome oxidase stripes of area 18 in the squirrel monkey. J Neurosci 7:3371–3377
Lund JS (1973) Organization of neurons in the visual cortex, area 17, of the monkey (*Macaca mulatta*). J Comp Neurol 147:455–496
Lund JS, Hendrickson AE, Ogren MP, Tobin EA (1981) Anatomical organization of primate visual cortex area VII. J Comp Neurol 202:19–45
Lund JS, Lund RD, Hendrickson AE, Bunt AH, Fuchs AF (1975) The origin of efferent pathways from the primary visual cortex, area 17, of the macaque monkey as shown by retrograde transport of horseradish peroxidase. J Comp Neurol 164:287–304
Maunsell JH, Van Essen DC (1983) The connections of the middle temporal visual area (MT) and their relationship to a cortical hierarchy in the macaque monkey. J Neurosci 3:2563–2586
Meskenaite V (1997) Calretinin-immunoreactive local circuit neurons in area 17 of the cynomolgus monkey, *Macaca fascicularis*. J Comp Neurol 379:113–132
Meyer HS, Schwarz D, Wimmer VC, Schmitt AC, Kerr JND, Sakmann B, Helmstaedter M (2011) Inhibitory interneurons in a cortical column form hot zones of inhibition in layers 2 and 5A. Proc Natl Acad Sci 108:16807–16812
Mullen RJ, Buck CR, Smith AM (1992) NeuN, a neuronal specific nuclear protein in vertebrates. Development 116:201–211

Nhan HL, Callaway EM (2012) Morphology of superior-colliculus- and middle temporal area-projecting neurons in primate primary visual cortex. J Comp Neurol 520:52–80

Pistorio AL, Hendry SH, Wang X (2006) A modified technique for high-resolution staining of myelin. J Neurosci Methods 153:135–146

Povysheva NV, Zaitsev AV, Kröner S, Krimer OA, Rotaru DC, Gonzalez-Burgos G, Lewis DA, Krimer LS (2007) Electrophysiological differences between neurogliaform cells from monkey and rat prefrontal cortex. J Neurophysiol 97:1030–1039

Povysheva NV, Zaitsev AV, Rotaru DC, Gonzalez-Burgos G, Lewis DA, Krimer LS (2008) Parvalbumin-positive basket interneurons in monkey and rat prefrontal cortex. J Neurophysiol 100:2348–2360

Preuss TM (2001) The discovery of cerebral diversity: an unwelcome scientific revolution. In: Falk D, Gibson KR (eds) Evolutionary anatomy of the primate cerebral cortex. Cambridge University Press, Cambridge, pp 138–164

Renier N, Wu Z, Simon DJ, Yang J, Ariel P, Tessier-Lavigne M (2014) iDISCO: a simple, rapid method to immunolabel large tissue samples for volume imaging. Cell 159:896–910

Rockel AJ, Hiorns RW, Powell TPS (1980) The basic uniformity in structure of the neocortex. Brain 103:221–244

Rockland KS, Pandya DN (1979) Laminar origins and terminations of cortical connections of the occipital lobe in the rhesus monkey. Brain Res 179:3–20

Rudy B, Chow A, Lau D, Amarillo Y, Ozaita A, Saganich M, Moreno H, Nadal MS, Hernández-Pineda R, Hernández-Cruz A, Erisir A, Leonard C, Vega-Saenz de Miera E (1999) Contributions of Kv3 channels to neuronal excitability. Ann N Y Acad Sci 868:304–343

Saleem KS, Logothetis NK (2007) A combined MRI and histology atlas of the rhesus monkey brain in stereotaxis coordinates. Academic Press, London

Sherwood CC, Raghanti MA, Stimpson CD, Bonar CJ, deSousa AA, Preuss TM, Hof PR (2007) Scaling of inhibitory interneurons in areas V1 and V2 of anthropoid primates as revealed by calcium binding protein immunohistochemistry. Brain Behav Evol 69:176–195

Shi SR, Key ME, Kalra KL (1991) Antigen retrieval in formalin-fixed, paraffin-embedded tissues: an enhancement method for immunohistochemical staining based on microwave oven heating of tissue sections. J Histochem Cytochem 39:741–748

Shipp S, Zeki S (1985) Segregation of pathways leading from area V2 to areas V4 and V5 of macaque monkey visual cortex. Nature 315:322–324

Shipp S, Zeki S (1989) The organization of connections between areas V5 and V2 in macaque monkey visual cortex. Eur J Neurosci 1:333–354

Shipp S, Zeki S (1995) Segregation and convergence of specialized pathways in macaque monkey visual cortex. J Anat 187:547–562

Soares D, Goldrick I, Lemon RN, Kraskov A, Greensmith L, Kalmar B (2017) Expression of Kv3.1b potassium channel is widespread in macaque motor cortex pyramidal cells: a histological comparison between rat and macaque. J Comp Neurol 525:2164–2174

Spatz WB, Tigges J, Tigges M (1970) Subcortical projections, cortical associations, and some intrinsic interlaminar connections of the striate cortex in the squirrel monkey (Saimiri). J Comp Neurol 140:155–174

Srinivasan S, Carlo CN, Stevens CF (2015) Predicting visual acuity from the structure of visual cortex. Proc Natl Acad Sci 112:7815–7820

Tootell RB, Taylor JB (1995) Anatomical evidence for MT and additional cortical visual areas in humans. Cereb Cortex 5:39–55

Turner EC, Young NA, Reed JL, Collins CE, Flaherty DK, Gabi M, Kaas JH (2016) Distribution of cells and neurons across the cortical sheet in Old World macaques. Brain Behav Evol 88:1–13

Valverde F (1978) The organization of area 18 in the monkey. Anat Embryol 154:305–334

van Brederode JFM, Mulligan KA, Hendrickson AE (1990) Calcium-binding proteins as markers for subpopulations of GABAergic neurons in monkey striate cortex. J Comp Neurol 298:1–22

Vickers JC, Huntley GW, Edwards AM, Moran T, Rogers SW, Heinemann SF, Morrison JH (1993) Quantitative localization of AMPA/kainate and kainate glutamate receptor subunit immunoreactivity in neurochemically identified subpopulations of neurons in the prefrontal cortex of the macaque monkey. J Neurosci 13:2962–2992

Vigneswaran G, Kraskov A, Lemon RN (2011) Large identified pyramidal cells in macaque motor and premotor cortex exhibit "thin spikes": implications for cell type classification. J Neurosci 31:14235–14242

von Bonin G, Bailey P (1947) The neocortex of Macaca mulatta. University of Illinois Press, Urbana

von Economo C (1927) Zellaufbau der Grosshirnrinde des Menschen. Verlag Julius Springer, Berlin. English edition: von Economo C (1927) Cellular structure of the human cerebral cortex (trans: Triarhou LC). Karger, Basel

Wang L-Y, Gan L, Forsythe ID, Kaczmarek LK (1998) Contribution of the Kv3.1 potassium channel to high-frequency firing in mouse auditory neurones. J Physiol 509:183–194

Weiser M, Bueno E, Sekirnjak C, Martone ME, Baker H, Hillman D, Chen S, Thornhill W, Ellisman M, Rudy B (1995) The potassium channel subunit Kv3.1b is localized to somatic and axonal membranes of specific populations of CNS neurons. J Neurosci 15:4298–4314

Williams RW, Rakic P (1988) Three-dimensional counting: an accurate and direct method to estimate numbers of cells in sectioned material. J Comp Neurol 278:344–352

Wolf HK, Buslei R, Schmidt-Kastner R, Schmidt-Kastner PK, Pietsch T, Wiestler OD, Blümcke I (1996) NeuN: a useful marker for diagnostic histopathology. J Histochem Cytochem 44:1167–1171

Wong-Riley MTT (1974) Demonstration of geniculocortical and callosal projection neurons in the squirrel monkey by means of retrograde axonal transport of horseradish peroxidase. Brain Res 79:267–272

Wong-Riley M (1979) Changes in the visual system of monocularly sutured or enucleated cats demonstrable with cytochrome oxidase histochemistry. Brain Res 171:11–28

Yoshioka T, Levitt JB, Lund JS (1994) Independence and merger of thalamocortical channels within macaque monkey primary visual cortex: anatomy of interlaminar projections. Vis Neurosci 11:467–489

Zeki S, Shipp S (1989) Modular connections between areas V2 and V4 of macaque monkey visual cortex. Eur J Neurosci 1:494–506

Zeng H, Shen EH, Hohmann JG, Oh SW, Bernard A, Royall JJ, Glattfelder KJ, Sunkin SM, Morris JA, Guillozet-Bongaarts AL, Smith KA, Ebbert AJ, Swanson B, Kuan L, Page DT, Overly CC, Lein ES, Hawrylycz MJ, Hof PR, Hyde TM, Kleinman JE, Jones AR (2012) Large-scale cellular-resolution gene profiling in human neocortex reveals species-specific molecular signatures. Cell 149:483–496

Ziemba CM, Freeman J, Simoncelli EP, Movshon JA (2018) Contextual modulation of sensitivity to naturalistic image structure in macaque V2. J Neurophysiol 120:409–420

Ziemba CM, Perez RK, Pai J, Kelly JG, Hallum LE, Shooner C, Movshon JA (2019) Laminar differences in responses to naturalistic texture in macaque V1 and V2. J Neurosci 39:9748–9756